# IDENTIFICATION AND CLASSIFICATION OF GREEN CITRUS BY SPECTRAL CHARACTERISTICS FOR PRECISION AGRICULTURE

By

KEVIN EDWARD KANE

A THESIS PRESENTED TO THE GRADUATE SCHOOL
OF THE UNIVERSITY OF FLORIDA IN PARTIAL FULFILLMENT
OF THE REQUIREMENTS FOR THE DEGREE OF
MASTER OF ENGINEERING

UNIVERSITY OF FLORIDA

2007

To my loving wife for all her support

ACKNOWLEDGMENTS

First I would like to thank my major advisor, Dr. Won Suk “Daniel” Lee, for his support and encouragement, both in my research and in my life. I would also like to give thanks to my other supervisory committee members, Dr. Thomas Burks and Dr. Arnold Schumann, for their advice and suggestions during my research. My family and friends were a great help and sustained through the good and bad times of this educational journey. Above all however, I would like to thank my wonderful and caring wife. I would surely not have pursued and finished graduate school without her by my side.

TABLE OF CONTENTS

page

LIST OF TABLES

LIST OF FIGURES

Abstract of Thesis Presented to the Graduate School
of the University of Florida in Partial Fulfillment of the
Requirements for the Degree of Master of Engineering

# IDENTIFICATION AND CLASSIFICATION OF CITRUS FRUIT BY SPECTRAL CHARACTERISTICS FOR PRECISION AGRICULTURE

By

Kevin Edward Kane

August 2007

Chair: Won Suk "Daniel" Lee
Major: Agricultural and Biological Engineering

Citrus production is a multi-million dollar industry in the state of Florida. The crop's economic significance is the driving force behind current developments in precision agriculture technologies assuring citrus growers can minimize their costs, protect the environment, and increase overall yield. A real-time citrus yield map while the citrus fruit are still maturing provides information to growers, giving them time to be proactive at improving the groves growth and planning ahead for the harvest. Recent research has shown cameras a image processing techniques have the ability to identify and count orange citrus fruit in the grove. However, there is a desire by the industry to have citrus yield maps earlier in the growing season, a time when citrus fruit are green. In this case, a traditional visible spectral camera can not accurately identify green citrus fruit against their green tree canopy.

The objective of this research was to use spectral information from the near infrared (NIR) reflectance spectrum to identify citrus fruit while they are still green. To begin this work, 540 freshly harvested samples of green citrus fruit and leaves were gathered and measured their diffuse reflectance using a spectrophotometer. The resulting spectral curves from 400 nm to 2500 nm were analyzed using discriminability calculations to find critical wavelengths for separation. Fisher linear discriminant analysis showed the wavelengths of 881 nm and 1383 nm

provided perfect green leaf and green fruit separation. This research provided a foundation for the design of an in-field NIR camera system for green citrus fruit identification.

A highly sensitive NIR camera outfitted with three optical band pass filters (1064 nm, 1150 nm, and 1572 nm) were used for natural in-field image acquisitions. The 256 bit monochromatic images were studied using spectral indexing and image processing schemes. Using training images, an indexing and image processing algorithm was developed and tested on validation images. A 90.3 % correct pixel classification result was obtained, proving that NIR camera images can successfully be used in the identification of green citrus fruit in the grove. An $R^2$ of 0.746 for fruit pixel counts verse a manually masked fruit pixel counts was achieved. Despite these positive accomplishments, the research has also revealed problems that are prohibitive to this identification method. These problems included the high financial cost of an NIR imaging system and the difficulty of proper illumination and multiple image alignments when working in a normal Florida citrus grove environment.

# CHAPTER 1
# INTRODUCTION

## Florida Citrus

Florida was first introduced to citrus in the 16th century by European explorers; with the first commercial production of citrus beginning in 1763. Over the next two centuries the citrus industry grew to a peak of over 350,000 ha of citrus in Florida (Sevier and Lee, 2003). In 2002, there were 322, 658 ha of commercial citrus groves spread throughout Florida, accounting for more than 74% of the total citrus grown in the United States. Among the citrus fruit varieties, the orange accounted for 81.4% of the production, followed by grapefruits at 13.2%, and other specialty fruits (tangerines, tangelos, lemons, limes, etc.) making up the last 5.4%. (Florida Agricultural Statistics Services [FASS], 2005) With an "on-tree" value of citrus estimated to be $1.1 billion in 2005 (Florida Agricultural Statistics Services [FASS], 2005), the citrus market has become extremely important to Florida's economy.

Currently international trade is putting pressure on the Florida citrus market. Cheaper labor in other countries, such as Brazil, has made the cost of staying competitive in the United States difficult for many growers. The need to increase yield per acre while lowering overall production costs is vital to the survival of the Florida Citrus industry. It appears that through technology and smarter grove management techniques like precision agriculture, the citrus industry will continue to thrive.

## Precision Agriculture in Florida Citrus

Traditional whole field management approaches treat the entire crop production area in a uniform manner ignoring natural in-field variability. This can lead to under or over application of field inputs at different locations. Precision agriculture is a managerial technique of using high-tech equipment to monitor and then treat smaller sections of a larger area on a site-specific

basis. This entails managing inputs (fertilizer, limestone, herbicide, insecticide, seed, etc.) to the farming land based on the variability inherent in the field. The goals of precision agriculture are to reduce waste, increase profits, and maintain the quality of the environment (Morgan and Ess, 2003).

Due to the "input-intensive" nature of citrus production and Florida's volatile trend of cost per unit area, precision agriculture is becoming a vital technique to manage the cost of production (Sevier and Lee, 2003). The Florida citrus production industry lends itself "perfectly" to the saving that can come from managing and controlling expensive inputs to the grove. Cost of production from input applications can be brought to "manageable" levels by precision agriculture. In addition to minimizing input costs, precision agriculture offers better managed groves, a protected environment, and increased crop yield and profits. Proper implementation of a precision agricultural system requires knowledge of in-field variability; in the case of this research, in-field citrus yield variability.

**Research history and trends**

According to the Citrus Research and Education Center (CREC) at the University of Florida, in early 1996 a meeting between citrus industry personal and the University of Florida's Institute of Food and Agricultural Sciences (IFAS) was held to discuss "decision support systems for citrus". This meeting resulted in the creation of the Decision Information Support System for Citrus (DISC) group at the CREC in Lake Alfred, FL. The goal of this group was to pursue research in the area of precision agriculture, with an emphasis on: mapping citrus yield, canopy volume, variable rate application and uses of the Global Positioning System (GPS) and geographic information systems (GIS) in commercial groves. This group's research has lead to advancements in precision citrus grove technologies and numerous published papers over the past decade.

Sevier and Lee (2003 and 2004) investigated Florida citrus growers' adoption of new technologies, including: sensor-based variable rate applicators, prescription map based variable rate applicators, pest scouting/mapping, GPS, soil variability mapping, water table monitoring, and yield monitoring and mapping. Their findings showed the most commonly used precision agriculture technologies were sensor-based variable rate applicators and soil variability mapping at usage rates of 18.6% and 18.0%, respectively (Sevier and Lee, 2003). The least used technology was remote sensing data from plane or satellite images, with a usage rate of just over four percent. Findings also showed that grower's age had a negative correlation with their likelihood of incorporating the technologies investigated (Sevier and Lee, 2004). That is younger growers were more likely to adopt the new technologies than older growers. This can be understood in a social realm by the younger grower being quicker to learn and use the computer technologies they have grown up with. The study also showed growers with higher "in-grove variability" are more likely to adopt new technology when compared to growers with less variability in their field.

In the Sevier and Lee survey (2004), respondents were asked to provide a reason for not adopting all new technologies. The leading reason for none adoption was that growers were "satisfied with current practices". They also described themselves as being somewhat reluctant to adopt, and "normally wait to see other's success" before implementing new technologies. These trends show the Florida citrus industry is moving slowly in the direction of new technologies, while continued research at the university level is needed to show growers the "success" they desire before adoption.

**Yield monitoring and mapping**

Knowledge of variable yields within blocks of citrus groves may provide information that a grower can use to find the cause of the variability (Whitney et al., 1998). There are many

elements within a grove or block that can lead to variability, including tree sizes, age, health, spacing, soil type, fertility, water availability, fertilizer application, and more. With proper knowledge of the variability in the field, grove managers may act not only in the right locations but also in a timely manner.

Fruit yield monitoring techniques may offer benefits for forecasting the number of fruit and quality at the time of harvest. Apple yield information together with ecological, cultivar, and price parameters can predict future yields, which in turn allows management to plan for incomes and calculations of profit (Welte, 1990). The European apple and pear industry only uses the 'Prognosfruit' Forcasting Model for their estimations of yield quantity and quality; however, this is a long tedious process requiring counting measurements of required parameters. This also limits the ability to predict individual orchards' future yields (Winter, 1986; Stajnko et al., 2004). Similarly, future citrus grove forecasting systems will also require yield quantity and quality parameters. Thus, the Florida citrus industry, like the European apple and pear industry will benefit from the use of fruit yield monitoring systems.

There have been several yield monitoring and mapping concepts proposed but few have found their way to actual development and field research. For the most part these systems can be grouped into three basic methods: 1) counting and mapping citrus tubs during manual harvesting 2) tracking citrus flow during mechanical harvesting, and 3) using automated computer vision systems before harvesting.

Citrus grove yield maps can be created during manual harvesting by marking the locations of filled tubs of fruit with a GPS unit in the grove (Whitney et al., 1998). This discrete data can be interpolated to create two dimensional yield maps. Using this method, yield maps can provide more meaning to growers by being presented in a boxes/acre format. DISC's early work

was with GeoFocus Inc, the only company at the time to offer a commercially available citrus yield monitoring system. Their Crop Harvest Tracking System (CHTS) required the truck operator to press a button 'marking' his/her GPS location every time a tube was lifted and emptied into a 'goat' truck. This seemingly easy system however had problems when operated with untrained or ill-informed drivers. Sometimes the operator would forget to push the button, or push the button multiple times just to be sure it was done. Other times the operator would remember to press the button later on, only after moving the truck location which means improper markings. All these button pushing mistakes diluted the data and resulting yield map's accuracy. Advancements to this system included automating the GPS system by way of a weight threshold switch on the truck's lifting arm and pressure transducers mounted on the 'goat' truck for weighing the citrus total (Whitney et al., 1999; 2001). Currently GeoAg Solutions located in Lehigh Acres, Florida, is the only company to provide citrus yield and monitoring solutions. They have incorporated more value added incentives with the technology such as monitoring worker progress, chemical applications and managing payments based on harvest counts.

GeoAg Solutions' main system is called CitriTrack with three additional sub-programs available: HaverstMap 2.0, HarvestPay, and HarvestWatch. The CitriTrack system can handle payroll, grove mapping, and tracks real-time harvesting progress. CitriTrack uses GPS and wireless technology to connect the grove manager directly to the grove. Up to date information is collected by a computer (also available for purchase) that is attached directly to the harvesting equipment. Similar to the GeoFocus system, the equipment operator logs each tub and its location and links it with the appropriate picker. HarvestMap 2.0 uses the yield data information collected from CitriTrack to produce informative full-color maps using GIS technology. GeoAg Solutions claim a grower can "track the daily progress in a block down to specific boxes, specify

variations within a block for chemical applications or even target and apply products based on return on investment potential". This data is collected in the field can also be routed to the HarvestPay software. The program tracks the information and can provide reports about worker productivity and hourly wages. The final sub-program, HarvestWatch, can allow the grove manager stay connected the crews with "up-to-the-minute reports" no matter their location.

A second method currently being explored is the use of fruit flow tracking technologies on mechanical citrus tree canopy 'shaker' harvesting equipment (Grift et al., 2006; Chinchuluun et al., 2007). Currently a canopy 'shaker' dislodges a citrus fruit from the canopy by violently shaking the citrus canopy. Freed citrus fruit can either fall to the ground and be harvested later by hand or the fruit can be caught by a conveyor mechanism, lifting the citrus up to a ramp where the citrus rolls down into a collection bin. Grift et al. (2006) have expanded previous research in estimating particle flow rates, more specifically fertilizer, by observing and measuring the space and time between "clumps" of particles. In this case, the "clumps and spacings" is measure by a laser and the particles are much larger and slower moving. Another more precise, but ultimately more complex solution, is counting the individual citrus by high speed cameras and using image processing techniques (Chinchuluun et al., 2007). Although current research is focused on fruit catching equipment working in conjunction with tree shakers, it should be noted that other forms of mechanized citrus harvesting equipment would produce even finer grade citrus grove yield maps, such as robotic citrus harvesting equipment. Such future systems could provide not only an exact count of fruit per tree, but also a size and quality of each fruit.

The final method explored for citrus yield map creation is the use of cameras with automated image processing and assessment techniques to count the number of citrus on tree.

By corresponding the image's citrus counts with their acquisition location in the grove by a GPS receiver, a highly detailed citrus yield map can be formulated. What separates this method from the pack is the availability of the yield map before the citrus is harvested. This provides time to grove managers to prepare more precisely the logistics of that harvested season and a head start at improving conditions for the following growing season. The research discussed throughout the remainder of this thesis is with respect to this on tree fruit counting citrus yield mapping method.

Agriculturally based vision systems have been used for the identification of everything from apples to weeds (Stajkno and Cmelik, 2005; Lee and Slaughter, 2004). On tree fruit identification using vision systems is not a new concept with original concepts dating back nearly forty years (Schertz and Brown, 1968). Research in fruit identification systems using machine vision have had mixed results with wide variations of camera systems, experimental tests, and image processing algorithms (Jimenez et al., 2000). Resent research at the University of Florida in the area of on tree citrus identification includes Annamalai et al. (2004), Chinchuluun and Lee (2006), and MacArthur et al. (2006). In these cases, a digital camera took visible light images of trees and then used image processing techniques to separate yellow/orange colors from the green canopies. In Chinchuluun and Lee's (2006) research, multiple cameras were used and the system was pulled behind a truck while passing through the grove rows. This allowed the images to be acquired from the side of the trees in high detail, which permitted morphological image processing techniques to work due to the closeness of the targets. MacAuthur et al. (2006) investigated the same concept but by using a remotely-piloted helicopter. This gave an advantage of flexible mobility throughout the grove, but additional skill was needed to gather high quality images. In both cases, citrus occlusion, shadows and the

separation of touching fruit were the most difficult problems faced. Research preformed on trees with different water treatment levels provided an interesting observation. The healthier the tree's canopy, the more difficult it was to count the fruit. A tree with thin or little leaf coverage made counting fruit easier and increasing the yield estimation, while a tree with healthy thick leaf coverage made the observation off all fruit imposable, thus low yield estimation (MacAuthur et al., 2006). It has been suggested that a weighted multiplier based on canopy fullness could be used to adjust these citrus yield estimations; however, no such work has been started at the time.

However, nearly every fruit finding vision system has used the visible light spectrum as the only means to decipher fruit from the surrounding leaf canopy. One resent exception was the promising work of Stajnko et al. (2004; 2005) using thermal imaging of apples, but there is no published work with citrus imaging outside the visible spectrum. A major consideration for the imaging of citrus is how the visible spectrum imaging research has only been preformed late in the growing season only after citrus has changed from a green to an orange color. A gap in citrus research is early season identification of citrus fruit, a time when the fruit is the same dark green color as the surrounding leaf canopy. Solving these problems can allow precision agricultural techniques to be used earlier in the growing season, thus compounding the benefits of early information on yield, health, and in-field variability.

# CHAPTER 2
# OBJECTIVES

## Identification of Critical Wavelengths

To properly identify and separate green citrus fruit from surrounding green citrus leaves using only near-infrared (NIR) spectral information, an investigation into the reflective characteristics was preformed. This involved the use of highly sensitive optical equipment to determine the spectral response of green citrus fruit and green citrus leaves in the visible to near-infrared range (VIS-NIR). Use of a statistically significant number of samples through the growing season provided large amounts of data to reliably analyze. It was the first objective of this research to identify the significant wavelengths needed to separate green citrus fruit from green citrus leaves in a controlled laboratory environment (Chapter 3).

## Green Fruit/Leaf Separation Using an NIR Camera

For future developments of early season citrus yield mapping systems, a test of in-field green citrus fruit/leaf separation was conducted in a Florida citrus grove using a highly sensitive NIR camera outfitted with optical band pass filters. Selection of the band pass filters was determined by the results of the first objective. The NIR camera's resulting monochromatic green citrus fruit and green leaf canopy images were post processed using image processing techniques. Differences in the spectral characteristics were the only image processing tools used for citrus identification. The second objective of this research was to determine if separation of green citrus fruit from green citrus leaves was possible in-field using current NIR camera and image processing technologies (Chapter 4).

# CHAPTER 3
# CITRUS CLASSIFICATION BASED ON DIFFUSE REFLECTANCE

## Introduction

Before designing a remote sensing camera system for the identification of green citrus in a green citrus leaf canopy, an in-depth study of the diffuse reflectance characteristics of green citrus and green citrus leaves was required. While the spectral responses of citrus leaves and citrus fruit had been studied many times in the past, the use of this information to find and identify a robust separation scheme in the near infrared (NIR) range had never been published. It was vital to identify critical wavelengths for separation, before proceeding with in-field camera research. It is only through the spectral characteristics that proper judgments could be made for the design and execution of the in-field NIR camera research.

## Literature Review

Research in the field of near infrared (NIR) sensing technologies on agriculture has been around for over a century. In most early research, the interactive nature between light and leaves was studied (Williams and Norris, 2001). It has been a more recent adaptation to incorporate NIR remote sensing equipment into the actual agricultural process, both pre and post harvest. This can be observed in the new technologies to track and monitor crop products and personnel (Whitney et al., 2001; Aleixos et al., 2002).

Citrus should be considered a late entry into the field of NIR sensing, despite the first major study on NIR diffuse reflectance of citrus fruit being three decades old (Gaffney, 1972). Since that research no real follow up work was conducted. Most likely this gap was due to two issues: 1) lack of valuable uses of the NIR technologies in the industry. Agriculture is among the slowest industries to research and adapt new technologies, as managers traditionally held a, “if it works don’t fix it” mentality (Sevier and Lee, 2003), and 2) the high cost of performing NIR

research in the past. Lower prices for better equipment and technologies are quickly eliminating these concerns for both the researchers and the eventual end users, the grove managers. Florida, and all U.S. citrus growers, will need to apply new managing solutions to compete with the growing international markets (Florida Agricultural Statistics Services [FASS], 2005). This means high-tech solutions are desired for pre-harvesting and post harvesting, resulting in the increase of NIR sensing research over the last decade.

Currently the most commonly used NIR technology in the agricultural fields of the world is multi- and/or hyper-spectral imagery from planes and satellites. This has lead to a lot of research in spectral vegetation indices (SVI) for finding a great number of important field information, such as disease, crop moisture, and weeds (Apan et al., 2003; Alchanatis et al., 2006; Gumz and Weller, 2005). Despite this, there has been little research preformed with these types of cameras and sensors on the ground. This research is a preliminary study of the reflectance characteristics of green citrus and green citrus leaves for the conceptual method design of a simple multi-spectral ground system, for separation of green citrus from green leave canopy.

## Materials and Methods

### Green Citrus and Green Leaves

During the fall 2005 citrus growing season, June 2005 to January 2006, samples consisting of one green citrus leaf and one green citrus fruit located next to each were acquired from the University of Florida's citrus research grove. A sample set consisted of 10 samples (10 fruits and 10 leaves) gathered on the same day and of the same variety. Sample sets were obtained weekly from one of the three citrus varieties: Hamlin (*Citrus sinensis*), "Orlando" Tangelo (*Citrus X tangelo*), and Valencia (*Citrus sinensis*). There were a total of 27 sample sets

collected: for a total of 270 individual fruits and 270 individual leaves. The dates and varieties of each harvesting sample set are listed in Table 3-1.

Table 3-1. List of dates that variety sample sets were harvested.

| Tangelo | Hamlin | Valencia |
|---|---|---|
| 7/6/05 | 7/12/05 | 10/18/05 |
| 7/19/05 | 7/26/5 | 11/1/05 |
| 8/2/05 | 8/23/05 | 11/22/05 |
| 8/9/05 | 9/7/05 | 12/6/05 |
| 8/16/05 | 9/20/05 | 12/20/05 |
| 8/30/05 | 10/5/05 | 1/3/06 |
| 9/14/05 | 10/19/05 | 1/11/06 |
| 9/27/05 | 11/2/05 | |
| 10/11/05 | 11/29/05 | |
| 10/25/05 | 12/13/05 | |

Figure 3-1 is an example of the green citrus and green leaves that were harvested during the growing season. Each sample was weighed to the nearest 1/100th of a gram by a digital scale (Adventurer, Ohaus, Inc., Pine Brook, NJ), and diameters (horizontally at the widest cross section with the stem pointing upwards) were measured using a sliding caliper to the nearest 1/100th of a millimeter on the same day as being harvested.

A   B

Figure 3-1. Samples from August 9, 2005 of A) green citrus fruit and B) green citrus leaf.

Figure 3-2 shows the citrus varieties growth during the fall season as measured by average width. Only ten citrus fruit samples were harvested every other week, or more, which allowed

the variance in average size to swing up and down. Close observation of Figure 3-2 even shows instances where the average size of the ten samples declined from the proceeding ten samples, such as Hamlin week two to week four. This was due to no other reason than the random nature of the fruit sizes harvested. The overall growth pattern, fruit sizes and seasonal developments are clear. Growth results, as measured by weight, showed similar results but have been excluded due to its irrelevance to the remainder of this thesis.

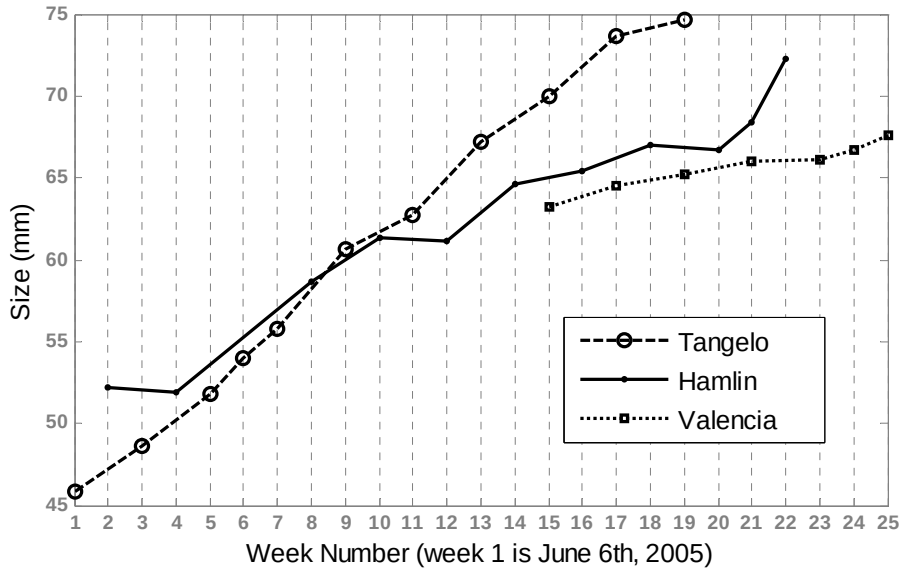


Figure 3-2. Growth chart of the average fruit varieties' size, as measured by fruit diameter.

**Diffuse Reflectance**

Diffuse reflectance of the leaf and fruit samples was measured by a spectrophotometer (Cary 500, Varian, Inc., Palo Alto, CA) with an integrating sphere (DRA-CA-5500, Labsphere, Inc., Brossard, Qc, Canada) on the same day as harvesting (Figure 3-3). The samples were not cleaned prior to measurements as natural "on tree" and "in-field" characteristics were desired. The spectrophotometer measured percent diffuse reflectance of the samples between 200 and 2500 nm in one nanometer increments. When the spectrophotometer was used, the two lamps (deuterium and tungsten) were allowed to warm up for one hour prior to testing to stabilize the

light sources. A diffuse reflectance baseline was measured using a 50 mm diameter polytetrafluoroethylene (PTFE) sample disk, which was used to obtain the optical reference standard for the system each day.

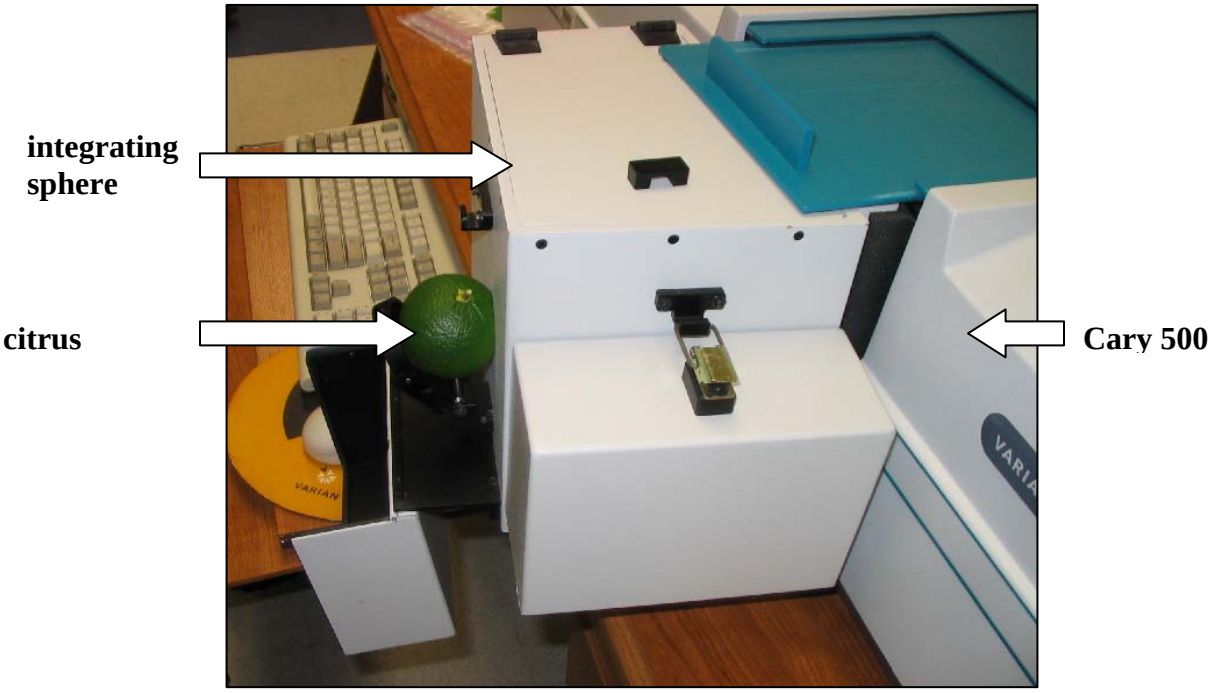


Figure 3-3. Green citrus fruit positioned for diffuse reflectance testing with the Cary 500 spectrophotometer with integrating sphere.

**Discriminability**

Two types of classification were desired from the data set. The most important was a distinction between citrus leaves and any citrus variety. This recognition would allow citrus growers to identify all immature green fruit regardless of variety. This information is critical as it offers transferable functionality to the research not only to local oranges and tangelos but also to limes, grapefruits and other members of the citrus family. The second classification studied the separation of citrus fruit into their variety classes: Tangelo, Valencia, and Hamlin. There were normal minor spectral reflectance changes over the course of the six month growing season due to chemical and physical alterations within the fruits' peel, based on the research of Nagy et

al. (1977). However, for the purpose of this research a normal Gaussian distribution was assumed at each wavelength for the reflectance of all sample fruits and leaves. Histograms of all fruits and leaves for wavelengths of 1650 and 881 nm are shown in Figures 3-4A and B, respectively. These example wavelengths serve as a visual comparison of 'strong' and 'weak' discriminability.

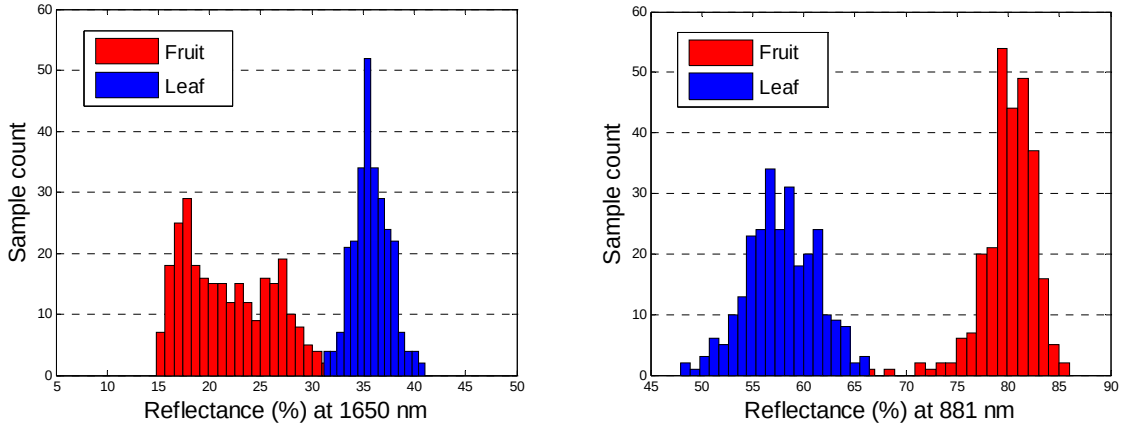


A B

Figure 3-4. Histograms of example fruit and leaf reflectance. A) Weak discriminability at 1650 nm. B) Strong discriminability at 881 nm.

Discriminability comprises two mathematical measures: the distance between means and the standard deviation of two probability density functions (PDFs). If we image the graphs from Figure 3-4 to be normalized and have an area under the curve of one unit, then Figure 3-4(A) shows a small overlap between the two PDFs, while Figure 3-4(B) shows a gap between the PDFs. This difference is a result of the discriminability of the two wavelengths.

The mathematical strength of the discriminability between two PDFs with the same standard distributions is defined by Duda et al. (1988) as:

$$d' = \frac{|\mu_2 - \mu_1|}{\sigma} \tag{3-1}$$

Where, $d'$ = discriminability

$\sigma$ = standard deviation

$\mu_1, \mu_2$ = means of class 1 and 2

In general, a higher discriminability value is desired as it shows a greater separation exists between classes. In the case of this data set, the standard deviations are different between the two classes, thus the formula above can not be used. For this reason the following alteration to equation 3.1 was made:

$$d' = \frac{|\mu_2 - \mu_1|}{(\sigma_1 + \sigma_2)/2} \tag{3-2}$$

Where, $d'$ = discriminability

$\sigma_1, \sigma_2$ = standard deviations of class 1 and 2

$\mu_1, \mu_2$ = means of class 1 and 2

Averaging the standard deviations of the two classes and replacing this for the standard deviation of equation 3.1 allows the discriminability to scale with the standard deviation change of both PDFs.

Discriminability is a simple and reliable way to determine which wavelengths have the greatest possible separation; however, this should not be the only consideration. Reflectance characteristics at one wavelength share common properties with those wavelengths near it. To maximize the quality of multiple feature extraction, a limit on the minimal distance between two wavelength features was set. This threshold limit will be defined in the Training and Validation section that follows.

**Fisher Linear Discriminant Analysis (FLDA)**

Dimensionality reduction is an issue with many recognition systems using more than one variable. The most well known and commonly used dimension reduction technique is principal component analysis (PCA). This method searches for feature spaces in the multi-dimensional

data that contains the greatest separation between classes with regard to variance. By projecting multi-dimensional data points onto a new calculated space, a smaller number of dimensions maybe used for classification. In the case of two dimensional data, a one dimensional direction is found. Fisher linear discriminant analysis (FLDA) is a common type of PCA first seen in the famous paper by Fisher (1936). In our research the analysis technique was used to calculate the direction, **w**, for projection. Duda et al. (1988) defines **w** as the "linear function yielding the maximum ratio of between-class scatter to within-class scatter". A positive byproduct of this analysis technique is a reduction of "noisy" directions. A one-dimensional projection direction was calculated, reducing data from a two dimensional space, defined by two feature wavelengths, to a one dimensional space. This methodology was chosen for this research as it adapts well to future NIR computer vision and image processing research. By using this method a stack of digital images at different spectral bands, know as a spectral image cube, can be dimensionally reduced to a single two dimensional image. Each pixel of this image would have its own uniquely calculated class likelihood.

**Training and Validation**

Prior to using the pattern recognition techniques discussed previously, a performance evaluation was conducted using two-thirds of the samples as training data and one-third as validation data. The 180 fruit and leaf training samples were selected at random. Using only the training samples, wavelengths for separation were selected, by discriminability as was discussed previously. FLDA was then used to find the best projection vector (direction). The remaining 90 fruit and leaf validation samples were classified after being projected onto the one dimensional space. Only the discrimination between fruit and leaf was verified using these techniques, as it was the primary purpose of the research.

For fruit vs. leaf classification, two methods (Method I and Method II) were investigated. Method I included the use of the feature wavelengths with the two highest discriminability (*d'*) calculations that also met a threshold distance of 100 nm apart. This 100 nm threshold was chosen arbitrarily to remove multicolinearity. Thus, the two selected wavelengths were allowed anywhere in the spectral range as long as they remained 100 nm apart. Method II required one wavelength feature having a fruit reflectance greater than that of the leaf, while the second wavelength feature having the fruit reflectance less than that of the leaf. The reader might be best served to glance over Figure 3-5 of the next page to better understand Method II. This second method was tested for fruit and leaf classification as it offered wavelengths with contrasting reflectance magnitudes.

## Results

### Reflectance Characteristics of Green Citrus Fruit vs. Green Citrus Leaves

Figure 3-5 presents the average reflectance spectra of 270 citrus samples with respect to the 270 leaf samples. From the spectral reflectance characteristic curves, two traits should be observed. The large increase of reflectance between 690 and 720 nm is referred to as the red edge. This is a result of plants having higher absorption rates in the visible range due to photosynthetic pigments. Absorption rates of the red edge region by chlorophyll pigments are lower resulting in higher reflectance (Ding, 2005). The second trait is water absorption bands at 970, 1450, and 1940 nm. These valleys in reflectance magnitude are a result of light absorption by water within the samples.

Differences between the fruit and leaf reflectance include a large magnitude change from 720 to 1120 nm. A simple experiment suggests this to be a result of the thickness of the citrus fruit compared to the thinness of the leaves. This was verified by stacking multiple leaves and testing the reflectance as the leaf count increased. The results showed that an increase in number

of leaves lead to an increased diffuse reflectance, most significantly between 720 and 1400 nm, as seen in Figure 3-6. This is explained as the first leaf's transmitted light may become a second leaf's reflected light. Thus, the more leaves the more opportunities there are to increase the reflectance (Figure 3-7). This theory is in agreement with Williams and Norris (2001) which preformed similar tests on thin potato slices. There were no significant increases in the reflectance due to leaf layering, outside this 720 to 1400 nm range. These results are supported by Fraser et al. (2002) which showed light penetration depths in apples was larger in the 700 to 900 nm range than 1400 to1600 nm. They claimed this to be a result of the absorption profile of water. A second important spectral difference between fruit and leaf in Figure 3-5 is the curve crossover occurring at near 1150 nm. All citrus varieties showed lower reflectance than the citrus leaves at higher wavelengths.

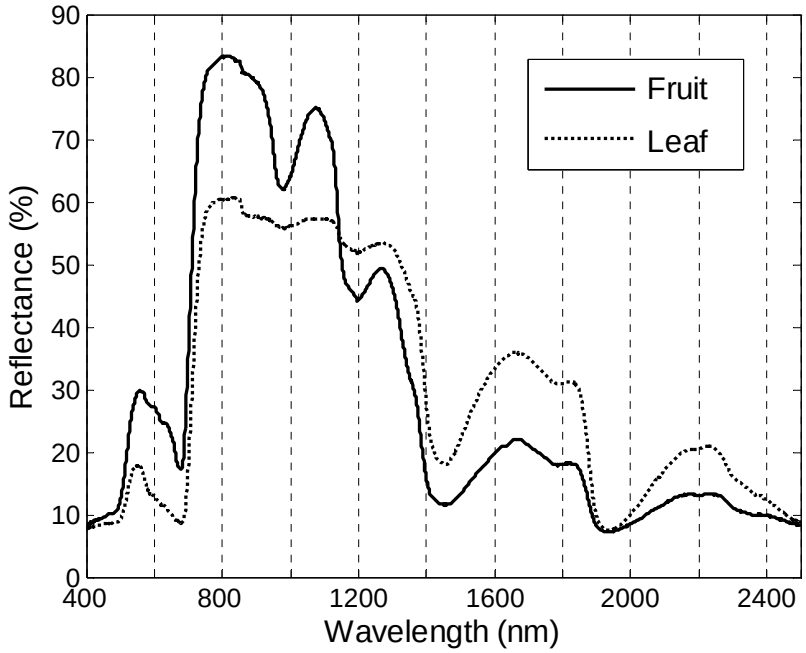


Figure 3-5. Green citrus and leaf average spectral reflectance through the fall 2005 growing season.

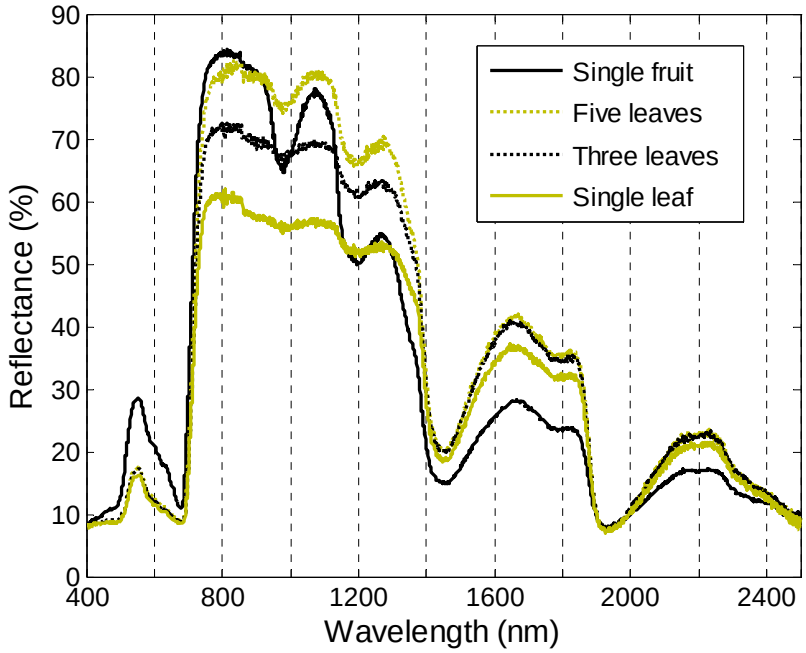


Figure 3-6. Spectral reflectance of layered citrus leaves and single "Orlando" Tangelo.

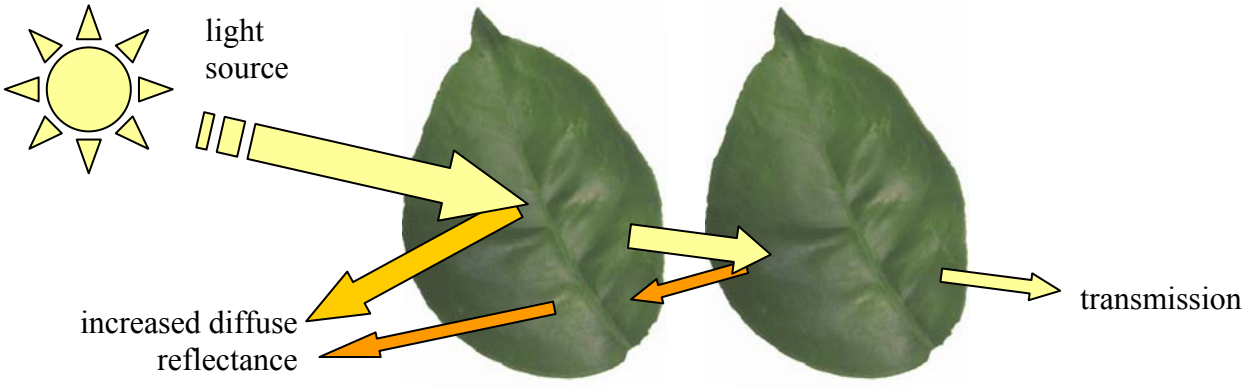


Figure 3-7. How multiple leaves/surfaces create added diffuse reflectance.

**Reflectance Characteristics of Citrus Varieties**

All three of the tested citrus varieties are highly correlated throughout the ultraviolet-visible (UV-VIS) to NIR range, as shown in Figure 3-8. It should be explained that the difference in the visible light range average, 400 to 750 nm, was a result of the fruits maturing during the experiment and the color brightness differences of those mature fruits. A difference in the chlorophyll to carotenoid conversion is the main cause of this color brightness (Merzlyak et

al., 1999). A consistent separation of citrus variety is seen in the diffuse reflectance magnitudes reflectance of the higher NIR spectral waves: Hamlin had the highest, followed by the Valencia and finally the Tangelo showing the lowest (Figure 3-9). Another way to view the separate of varieties is based on their individual standard deviations as compared to the standard deviation of all the citrus samples, presented in Figure 3-9. It shows the greatest standard deviation of all the varieties to be much higher in the spectral range of 1400 to 1880 nm with an additional standard deviation range maximum around 2200 nm. Meanwhile, the standard deviations' of the individual varieties remain low at those same wavelength ranges. This suggests that they are prime wavelengths for variety classifications information, a statement which will be mathematically proved later (Table 3-3). Note that the highest standard deviations are at 660 nm due to the color conversion mentioned before. Because the standard deviation of the individual citrus varieties remains high here as well, this would not be a good location to gather classification information.

The average reflectance of leaf varieties showed a maximum less than 3% separation. Those separations are insignificant when compared with standard deviations on the order of 3.5%, thus the leaf variety classification was not possible with our results.

The reflectance curves were converted to absorbance spectra by use of the Beer-Lambert law, Equation 3-3 (Williams and Norris, 2001) (Figure 3-10). Although analysis for light absorbance compared to absorber is not discussed in depth in this thesis, the reader should understand that light absorbance by materials is completely dependent on the molecular structures of the said material. More specifically the Beer-Lambert Law states, the concentration of an absorber is directly proportional to the sample absorbance (Williams and Norris, 2001). This fact is used throughout the agricultural and food industry in non-destructive examinations of

food. It should also be realized by the reader that the different absorbance curves of Figure 3-10 mean different absorber components and quantities exist among the citrus varieties.

$$A = \log\left(\frac{1}{R}\right) \tag{3-3}$$

Where, A = Absorbance and R = Reflectance

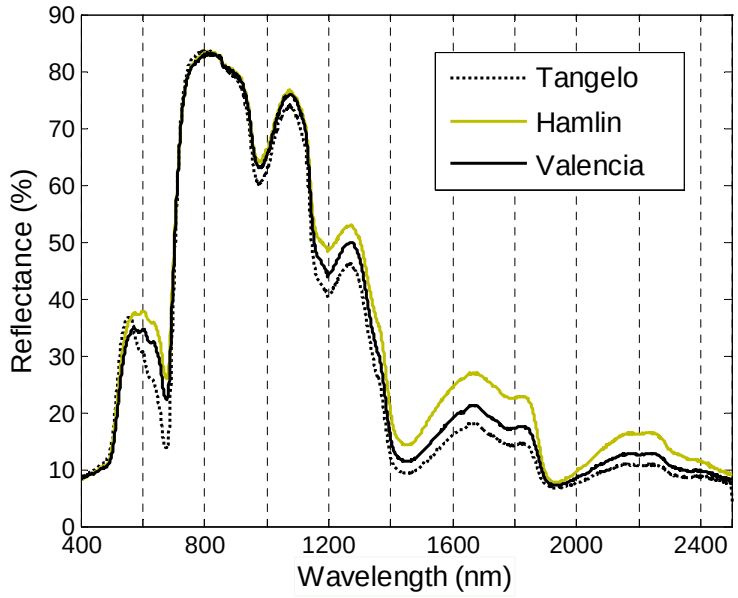


Figure 3-8. Citrus varieties average spectral reflectance.

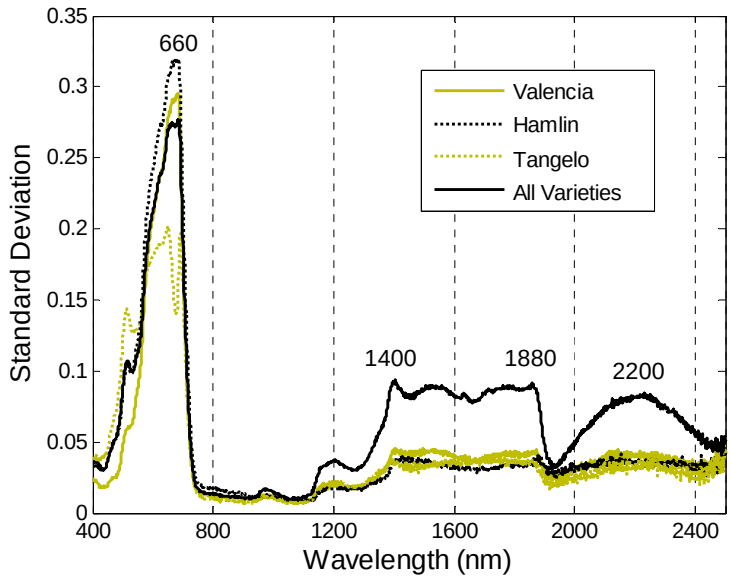


Figure 3-9. All citrus and citrus varieties standard deviation values for all wavelengths.

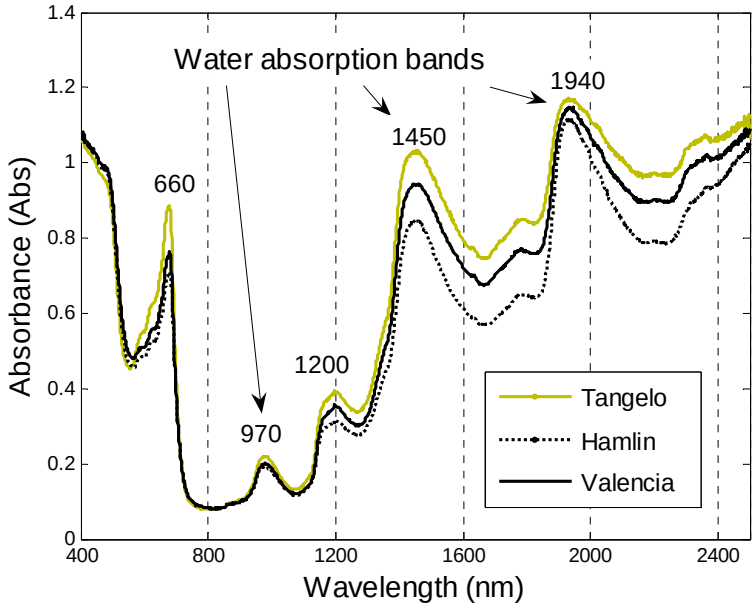


Figure 3-10. Citrus varieties average spectral absorbance.

**Spectral Growth Patterns of Maturing Citrus Fruit**

To verify that the chemical and biological changes occurring inside the maturing green citrus fruit would not significantly harm our identification methods, a brief survey of the spectral growth pattern was conducted. Previous research (Merzlyak et al., 1999) conducted on the maturing process of citrus focused mostly on identifying wavelengths signaling growth. In this research, sampling ranges that show growth are to be avoided, to prevent maturing from harming the accuracy of our identification. A solution that can identify both early season and end of season citrus offers more robustness and/or could be implemented other future citrus harvesting systems.

Changes to reflectance are dramatically illustrated in Figure 3-11, where early season Hamlin sets harvested on July 12, 2005 and September, 20 2005 are compared with later sets on November 2, 2005 and December 12, 2006. By mid December, 2005 Hamlin samples turned a bright orange. To design a machine vision system that identifies green or orange citrus fruit

from green citrus leaves, the 500 to 750 nm range needs to be avoided due to these dramatic spectral reflectance changes.

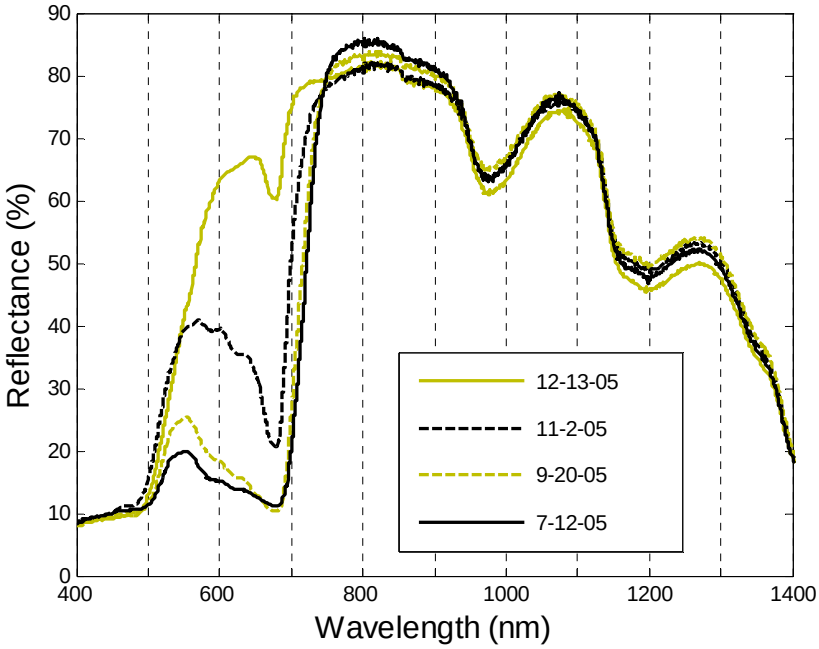


Figure 3-11. Reflectance changes over the growing season of Hamlin.

**Training and Validation Results**

Discriminability results of the training data set, Methods I and II are shown in Table 3-2. The training data shows separation between green citrus fruit and leaves to be the strongest at 863 nm, with a discriminability value of 7.84. The strongest separation wavelength based on discriminability that met the 100 nm distance threshold was 763 nm. The strongest wavelength for separation above 1150 nm, where leaf reflectance is greater than fruit reflectance, was 1389 nm. These second and third feature wavelengths, 763 and 1389 nm, respectively, show 'weaker' separation but are still relatively 'strong' for classification purposes.

Scatter plots of the validation data using Methods I and II are shown in Figures 3-12 and 3-13, respectively. Using a "classification line" passing through the centroid of the training data and perpendicular to the "projection line", all samples but one validation fruit were correctly

Table 3-2. Discriminability results of the training data set, Methods I and II.

| | Feature 1 | | Feature 2 | |
|---|---|---|---|---|
| | wavelength (nm) | discriminability, *d'* | wavelength (nm) | discriminability, *d'* |
| Method I | 863 | 7.84 | 763 | 6.72 |
| Method II | 863 | 7.84 | 1389 | 4.87 |

identified using Method I wavelengths, yielding $R^2 = 0.994$ (Figure 3-12). Using Method II wavelengths, all of the validation data was correctly identified, yielding $R^2 = 1.000$ (Figure 3-13). It can be observed that Method I of the fruit to leaf separation possesses the strongest discriminability values; however, the scatter plot of Method II displayed stronger separation in the two dimensional space, as shown in Figures 3-12 and 3-13.

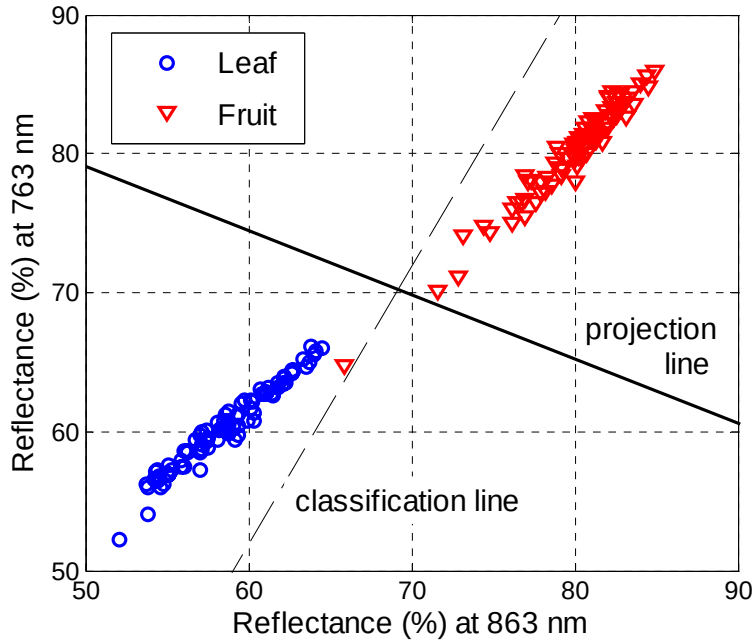


Figure 3-12. Fruit & Leaf (Method I) with Fisher projection line (solid line) and classification line (dashed line).

**Discriminability Using All Samples**

The discriminability results using all the samples data is shown in Figure 3-14. It is important to notice the general trend of this graph and what regions show the 'strongest' discriminability, 740 to 940, 1060, 1380, and 1570 to 1830 nm, and what regions have the

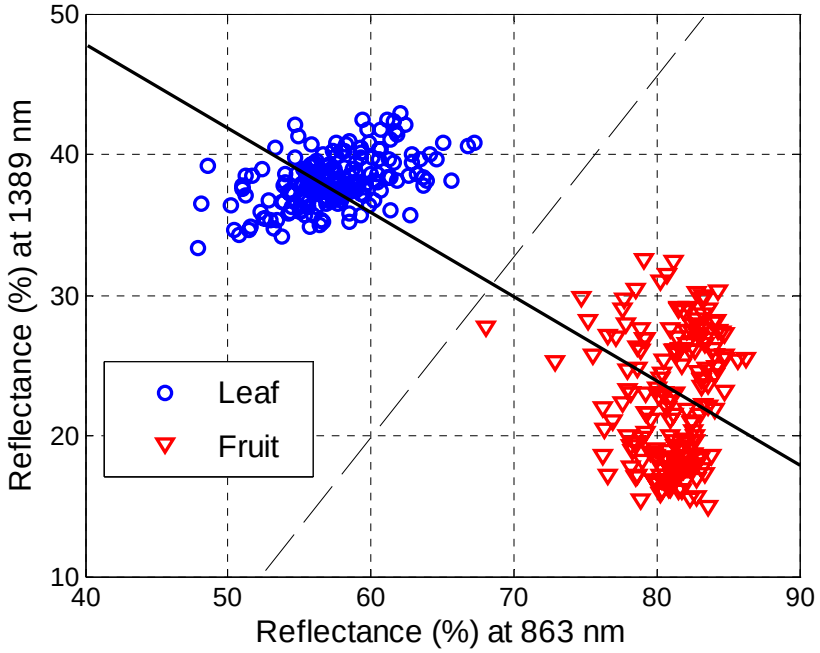


Figure 3-13. Fruit & Leaf (Method II) with Fisher projection line (solid line) and classification line (dashed line).

'weakest' discriminability, 1140, 1930, and 2500 nm. Although the remainder of the mathematical analysis in this Chapter is dependent on the randomly selected training and validation sets, this figure will be referenced back to in Chapter 4 in the selection of optical equipment.

The results of discriminability calculations using all samples are similar to the training data results, with the strongest discriminability at 881 nm. Using Method I gives the second feature wavelength at 781 nm while Method II gives 1383 nm, as shown in Table 3-3. Notice that 'weak' discriminability in wavelengths with high mean separations can be an artifact of the multi-modal nature inherent in the total fruit PDF, for example 1650 nm seen in Figure 3-4A. The difference between fruit variety reflectance increases the standard deviations at these wavelengths. The three peaks seen in the fruit histogram of Figure 3-4A serves as visual evidence of the three fruit varieties' multi-model effect.

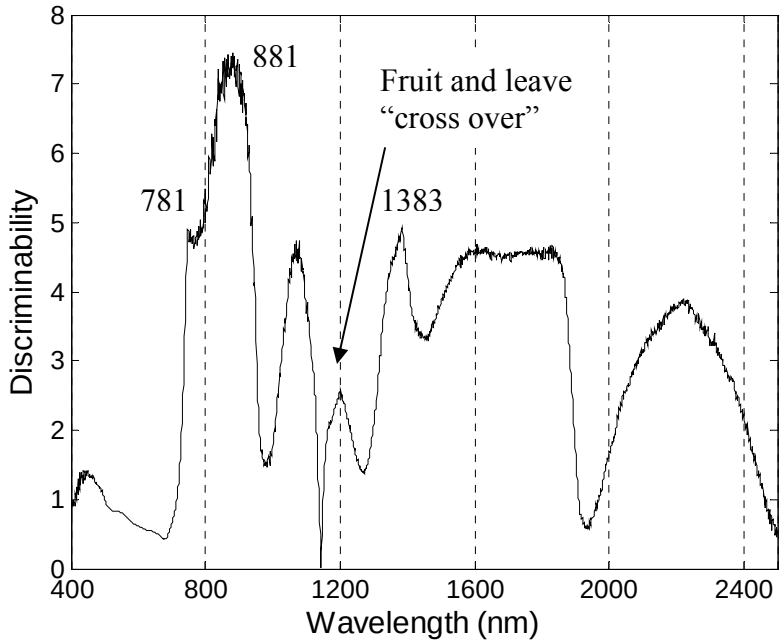


Figure 3-14. Discriminability results of all the sample citrus vs. leaves.

Table 3-3. Discriminability results using all the data.

| | Feature 1 | | Feature 2 | |
|---|---|---|---|---|
| | wavelength (nm) | discriminability, *d'* | wavelength (nm) | discriminability, *d'* |
| Fruit & Leaf (Method I) | 881 | 7.44 | 781 | 4.98 |
| Fruit & Leaf (Method II) | 881 | 7.44 | 1383 | 4.92 |
| Tangelo & Hamlin | 1712 | 5.52 | 1392 | 5.44 |
| Tangelo & Valencia | 1417 | 2.96 | 1882 | 2.83 |
| Hamlin & Valencia | 1711 | 3.20 | 1813 | 2.89 |

Figures 3-15, 3-16, and 3-17 show scatter plots created by the feature discriminability results in Table 3-3. When observing the fruit variety plots, most significantly Figure 3-15, the difficulty in using features with dependencies on each other are seen. The result is a class cluster of 'cigar shapes' with high variances in the same direction. Incase of Figure 3-15, the variance is between the bottom left corner and the top right corner of the graph. This can create difficulty

with class separations by means of PCA, due to the dependences of one feature space on the next.

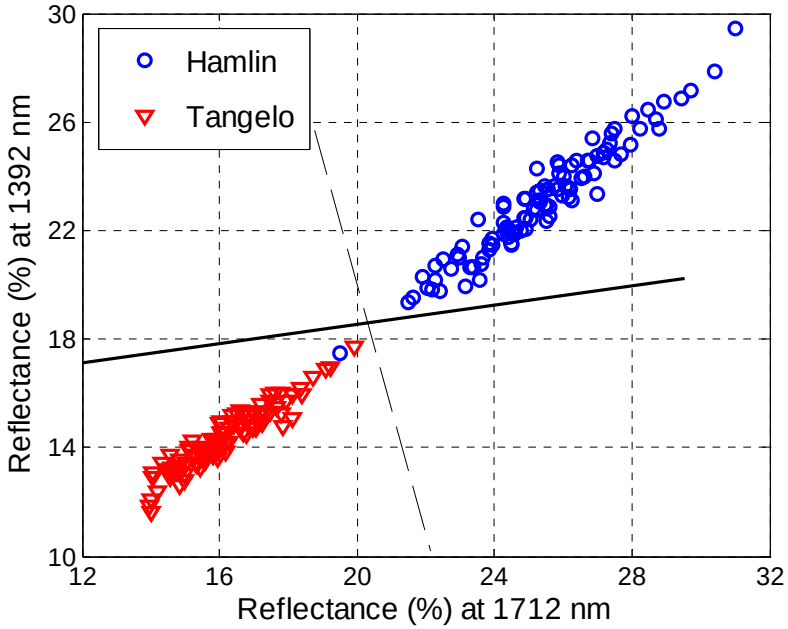


Figure 3-15. Tangelo & Hamlin with Fisher projection line (solid line) and classification line (dashed line).

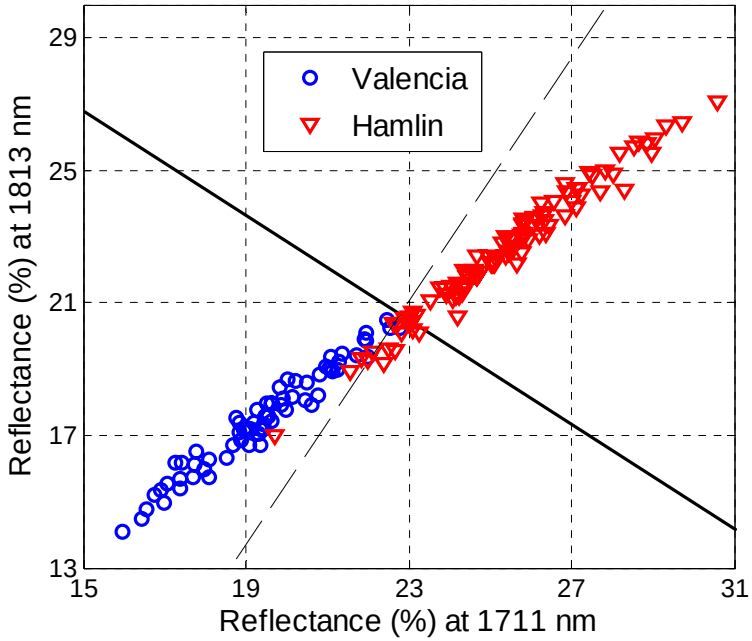


Figure 3-16. Tangelo & Valencia with Fisher projection line (solid line) and classification line (dashed line).

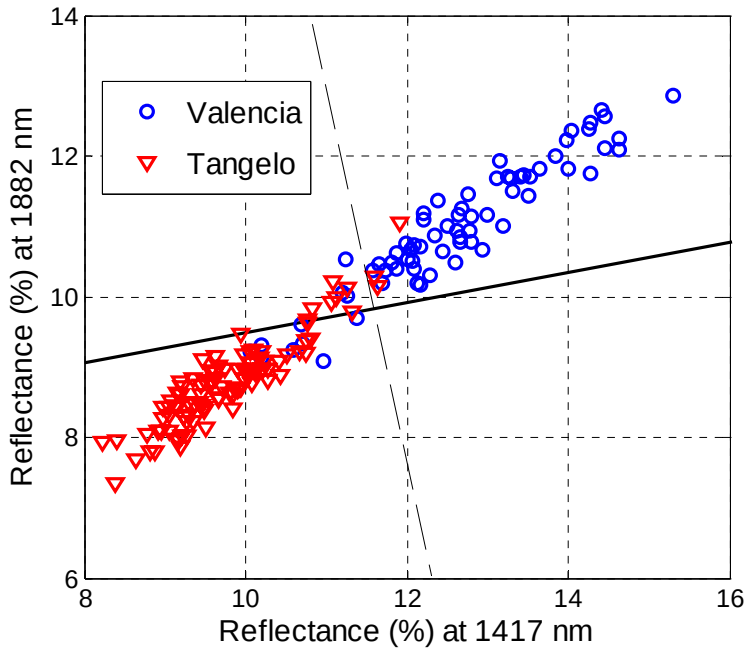


Figure 3-17. Hamlin & Valencia with Fisher projection line (solid line) and classification line (dashed line).

**Fisher Linear Discriminant Analysis (FLDA) Results**

The solid lines in Figures 3-12, 3-13, 3-15, 3-16 and 3-17, are the projection lines calculated by FLDA. While several of the calculated projection lines, **w**, are intuitively correct like Figure 3-13, others are counter intuitive such as Figure 3-16. The parallel nature of the two 'cigar shaped' class clusters is the cause of this odd looking projection line. The reasoning is that the class means of the projected data on to the one-dimensional space is close in distance; however, the "between-class scatter to within-class scatter" (Duda et al., 1988) is the best for the most accurate classification, because of a lower variance. A look back at Figure 3-12 is an example of the same tendency for the projection line to be perpendicular to 'cigar shaped' clusters.

Mathematical definitions of the calculated projection vectors for the two class systems are shown in Table 3-4. Notice the projection space is one dimensional and not defined by a line but

rather a direction; a line was included in the figures only as a visual reference. A complete scatter plot including all 270 data samples of every class is in Figure 3-18. The x-axis uses a feature wavelength of 881 nm as it displayed the strongest discriminability for fruit and leaf identification, while the y-axis uses a feature wavelength of 1713 nm as it displayed the strongest average discriminability between fruit varieties.

Table 3-4. Projection vector equations found by Fisher Linear Discriminant analysis

| | Feature 1 (x-axis) | Feature 2 (y-axis) | Projection vector, **w** |
|---|---|---|---|
| Fruit & Leaf (Method I) | 881 nm | 781 nm | **w** = ( -0.1309, 0.0439 ) |
| Fruit & Leaf (Method II) | 881 nm | 1383 nm | **w** = ( -0.0612, 0.0380 ) |
| Tangelo & Hamlin | 1712 nm | 1882 nm | **w** = ( -0.5119, -0.1092 ) |
| Tangelo & Valencia | 1417 nm | 1813 nm | **w** = ( -0.9040, 0.7114 ) |
| Hamlin & Valencia | 1711 nm | 1381 nm | **w** = ( -0.1751, -0.0312 ) |

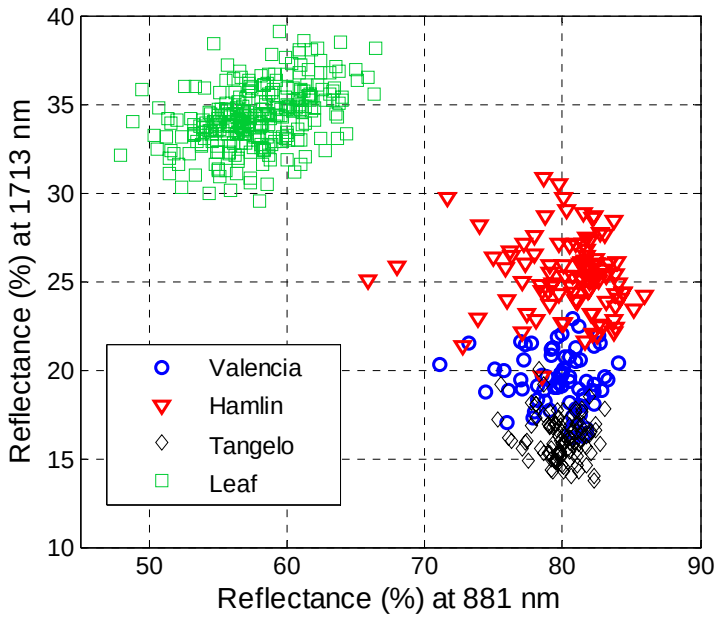


Figure 3-18. Scatter plot showing all classes: Valencia, Hamlin, Tangelo, and Leaf.

## Conclusions

Samples of green citrus varieties and citrus leaves were harvested during the late 2005 growing season. Diffuse reflectance over the UV-Vis and NIR range (200 to 2500 nm) was measured with a spectrophotometer. Average spectral reflectance curves show the opportunity to use NIR sensors and/or cameras to identify citrus fruit from citrus leaves, but also to classify different citrus varieties. Wavelength features for classifications were chosen by discriminability calculations. The selected feature spaces were used to create two dimensional scatter plots, which were then used to calculate the best projection line by Fisher linear discriminant analysis (FLDA). Using two-thirds of data as training and one-third data as validation, an $R^2$ of 1.0 was possible using these pattern recognition techniques. As expected, separating green leaves from green citrus fruit proved to be more accurate than distinguishing among different citrus varieties.

It has been shown in this Chapter that while using only two NIR feature wavelengths, extremely accurate green citrus fruit from green citrus leaf identification is possible. A scatter plot of feature wavelengths 881 nm (x-axis) and 1383 nm (y-axis) projected onto a one dimensional feature space defined by the direction (-0.0612, 0.0380) proved to be the best mathematical method for separation when using the data gathered in the laboratory. The transferability of these critical wavelengths and mathematical methods to in-field systems have some interesting difficulties to be discussed later.

This Chapter's research was designed to test NIR data validity for the use in a computer vision system for counting green citrus yield in-field, while still on the tree. The in-field testing of such a NIR camera based system is in the following chapter, Green Citrus Identification by a NIR Camera System (Chapter 4).

# CHAPTER 4
# CITRUS INDENTIFICATION BY NIR CAMERA SYSTEM

## Introduction

After completion of the spectral analysis of green citrus fruit and green citrus leaves, it was important to use that knowledge in the selection of optical camera equipment. The selection of wavelengths is of significance during image processing because an understanding of the expected spectral responses helps in spectral index designing and testing.

## Cameras Used in Citrus Yield Mapping

Fruit identification using machine vision systems was proposed nearly forty years ago (Schertz and Brown, 1968). However, technology has been only recently advanced enough to allow researchers to investigate their usefulness more fully. Major fruit identification studies have focused mostly on apples and citrus fruit, the most common application being robot harvesting (Jimenez et al., 2000). Traditionally the visible spectrum has been used for fruit identification, which lends itself very conveniently to non-green colored fruits, such as red apples and orange colored citrus. The biggest issues with these camera systems have been occlusion and grouped fruit segmentation (Jimenez et al., 2000).

Citrus harvesting system research has used cameras with different forms of traditional machine vision for many years with mixed results and a wide variation of algorithms (Jimenez et al., 2000). Recent research in this field of study at the University of Florida includes Annamalai et al. (2004), Chinchuluun and Lee (2006) and MacArthur et al. (2006). However, all of these systems utilized only the visible light spectrum as a means to decipher fruit from the surrounding green leaf canopy. This leads to problems with early season citrus identification, a time when citrus are a dark green color, the same color as the leaves. By solving this problem, precision

agricultural techniques can be used earlier in the growing season, compounding their benefits of early information on citrus fruit yield, health, and in-field variability.

Annamalai and Lee (2004) proposed a method to decipher green citrus fruits from leaves by their spectral differences in the near infrared (NIR) region. This work was extended in Chapter 3 by using a spectrophotometer to identify critical wavelengths that could be used to separate green citrus fruit from green citrus leaves. The objective was to test a simple non-destructive computer vision system for the identification of green citrus fruit while "on-tree" and during normal in-field growing conditions utilizing the previously obtained results of Chapter 3

## Materials and Methods

### NIR Camera, Optical Equipment, and Hardware

A Merlin NIR InGaAs camera (FLIR Systems, Inc., Indigo Operations; Wilsonville, OR) was used for all image acquisitions. The spectral range of this NIR camera is 900 to 1700 nm with the light sensitivity dropping off to zero at each side of this range and a peak sensitivity at approximately 1600 nm. This sensitivity curve is true of all InGaAs technology and is displayed in Figure 4-1, courtesy of FLIR, Inc. The Merlin NIR camera recorded 640 x 480 pixel monochromatic images (307200 pixels), saved in a two-dimensional grayscale TIFF format with 256 possible pixel values (0 to 255). Each image was taken with one of three optical band pass filters (1064, 1150, and 1572 nm) positioned in front of the camera lens, permitting only a thin spectral band of light to pass. Figure 4-2 shows the three optical band pass filters used during the image acquisitions of this study. Additional technical details about each band pass filter are provided in Table 4-1.

The two most critical wavelengths discovered and discussed in Chapter 3, for the separation of all green citrus varieties from green citrus leaves were those of Method II (i.e., 881 nm and 1383 nm). However, the spectral range of an NIR InGaAs camera starts at 900 nm, and

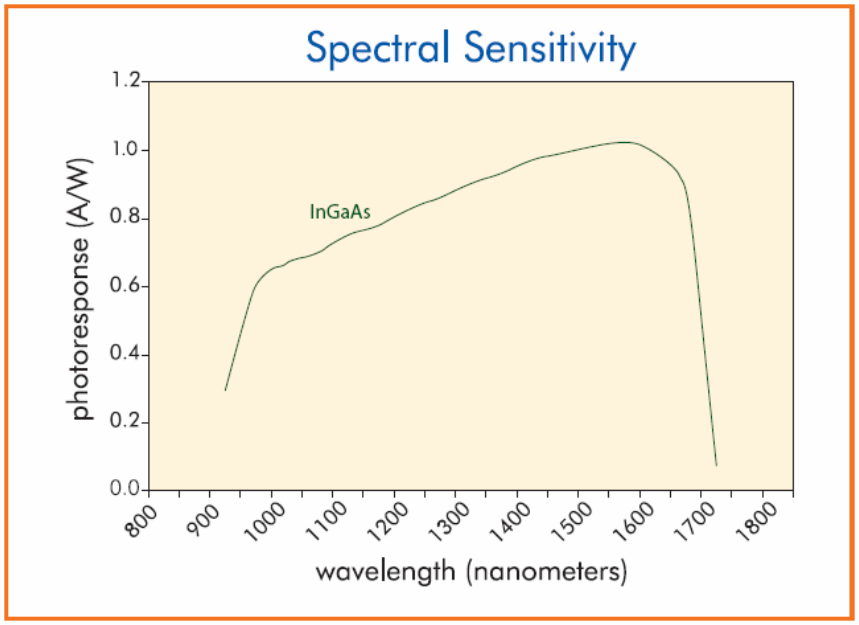


Figure 4-1. Spectral sensitivity range of InGasAs technology (Graph courtesy of FLIR Systems, Inc.).

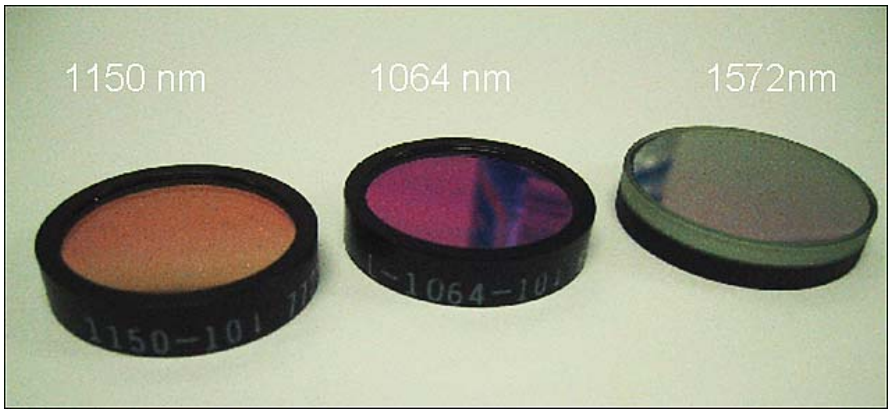


Figure 4-2. Three band pass (1150 nm, 1064 nm, and 1572 nm).

Table 4-1. Optical band pass filter details.

| Supplier/Manufacture | Model | CWL (nm) | FWHM (nm) | Transmittance |
|---|---|---|---|---|
| ThorLabs | FL1064-10 | 1064.0 | 10.0 | 70% |
| ThorLabs | FB1150-10 | 1150.0 | 10.0 | 45% |
| Andover | 1572.0 / 20.0 - 27539 | 1572.0 | 15.0 | 75% |

even at 900 nm the spectral sensitivity is very low, less than 20% of the maximum sensitivity range. Referring back to Chapter 3, the wavelength selection to best mimic the wavelength of strongest citrus fruit and leave separation is around 1060 nm. This was the reasoning for the selection of the FL1064-10 model with a central wavelength (CWL) of 1064 nm. The second band pass filter, model FB1150-10 has a CWL of 1150 nm and was selected because the wavelength had a low discriminability between citrus and leaf, making it ideal for normalizing images.

The final band pass filter was the 1572.0 / 20.0 with a CWL of 1572 nm. A filter selection of 1383 nm was not made fore two important reasons. One, no filter around 1383 nm is commercially available while maintaining a transmittance of over 50% and a full width half maximum (FWHM) value of less than 50 nm. Two, and far the most importantly, the spectral solar intensity between 1450 and 1350 nm is low, close to zero. It is desirable to use wavelengths of higher solar intensity to present the best lighting conditions possible (Figure 4-3). The range 1550-1590 nm provides the stronger solar intensity that is desired. Also referring to Figure 4-3 the spectral irradiance of 1064 nm is a strong 0.65 W $m^{-2}$ $nm^{-1}$, while the 1150 nm remains lower but still functional with a spectral irradiance at about 0.3 W $m^{-2}$ $nm^{-1}$.

Figure 4-4 shows spectrophotometer (Cary 500, Varian, Inc., Palo Alto, CA) transmittance results of the three band pass filters. The observation of most interest is the transmittable light bands outside each specific band pass filter design range (i.e., the 1064 nm band pass filter transmittance spikes at 800 nm, 1600 nm, and above; the 1572 nm band pass filter transmittance spikes at 1950 nm and above). Most of these extra band passes are limited by the NIR camera range of 900 to 1700 nm; however, the exception is the 1600 nm spike of the 1064 nm band pass

filter. While this was of some concern, it should be noted that the solar intensity at 1064 nm is greater than that of 1572 nm. As a result, the transmittance of the 1600 nm spike are overcome

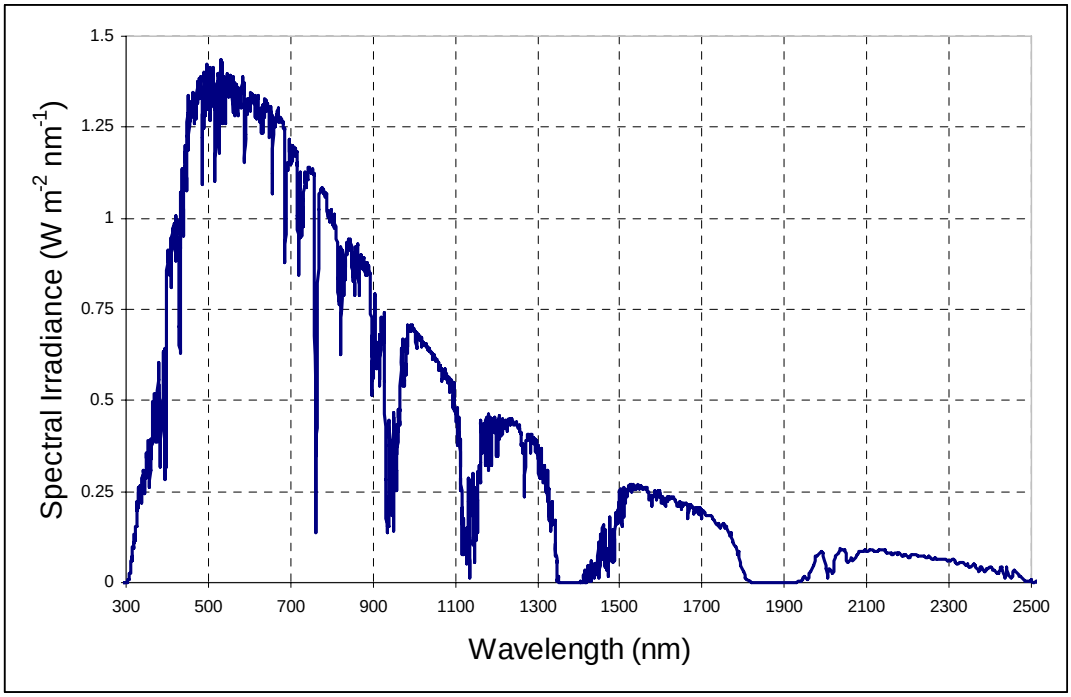


Figure 4-3. Solar spectral irradiance reference from the ASTM G173-03 of "direct circumsolar". This data was gathered by the American Society for Testing and Materials (ASTM) and government research laboratories.

by the stronger solar light at 1064 nm, having only a small effect on the resulting images. In contrast, the same transmittance levels for the 1572 nm band pass filter remain acceptable, because the NIR camera mechanical iris can be opened allowing enough of the 1570 nm solar light in. In fact, during image acquisition the iris was always opened more for the 1572 band pass filter imaging then for the other two filters. The band pass filters were all bi-directional with the same transmittances in both directions. Although this was verified by the spectrophotometer, the results shown in Figure 4-4 are from the same direction as was consistently used throughout the image acquisition process.

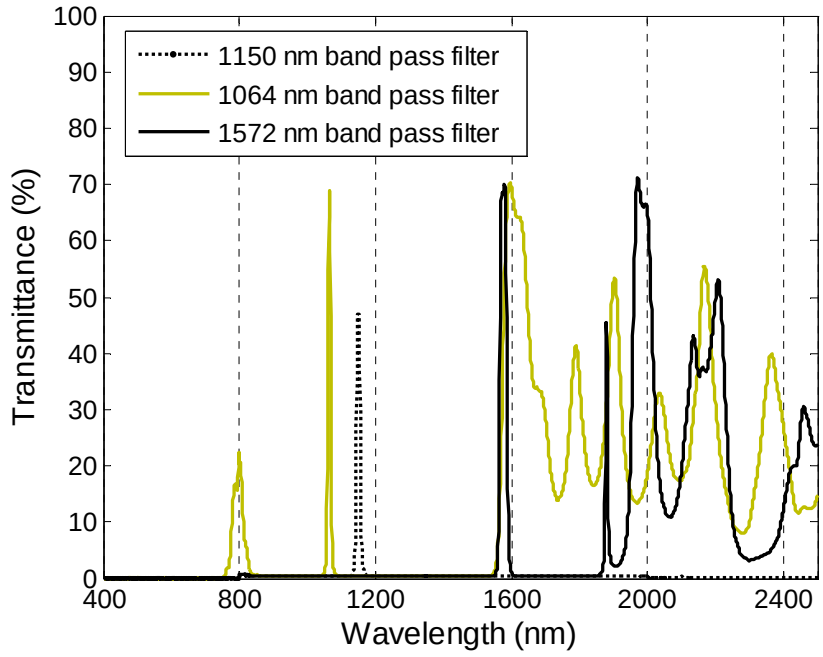


Figure 4-4. Percent transmittance for each of the band pass filters.

An in-field experimental setup used a gasoline generator to supply a standard North American wall outlet power supply of 120 Volts, peak-to-peak. The generator powered a computer monitor, the NIR camera, and a personal computer (Pentium 4, 2.4 GHz). The NIR camera was connected by coaxial cable to the PC, which was running image acquisition software (Intellicam, Matrox Electronic Systems Ltd., Dorval, Canada). The in-field experimental setup is shown in Figure 4-5. The use of a light weight table and wagon was to facilitate the easy moving of equipment from one image location to another.

**Experimental Location and Environment**

In order to acquire multispectral images, the NIR camera was positioned in front of citrus fruit and leaves and an optical band pass filter was manually locked into place in front of the lens. Images were taken before switching to the next optical filter without moving the NIR camera. Each time a filter was positioned, several images (three to seven) were obtained with the same filter. A commercial digital camera (Canon Digital Elph S300) was used to record a

visible spectrum image of the NIR camera field of view to be used later for target scene referencing. For the purpose of this thesis, an NIR camera field of view showing citrus fruit and leaves will be referred to as a "target"; a group of spectral images acquired at a target will be referred to as an "image", and a "raw image" will refer to a single monochromatic image.

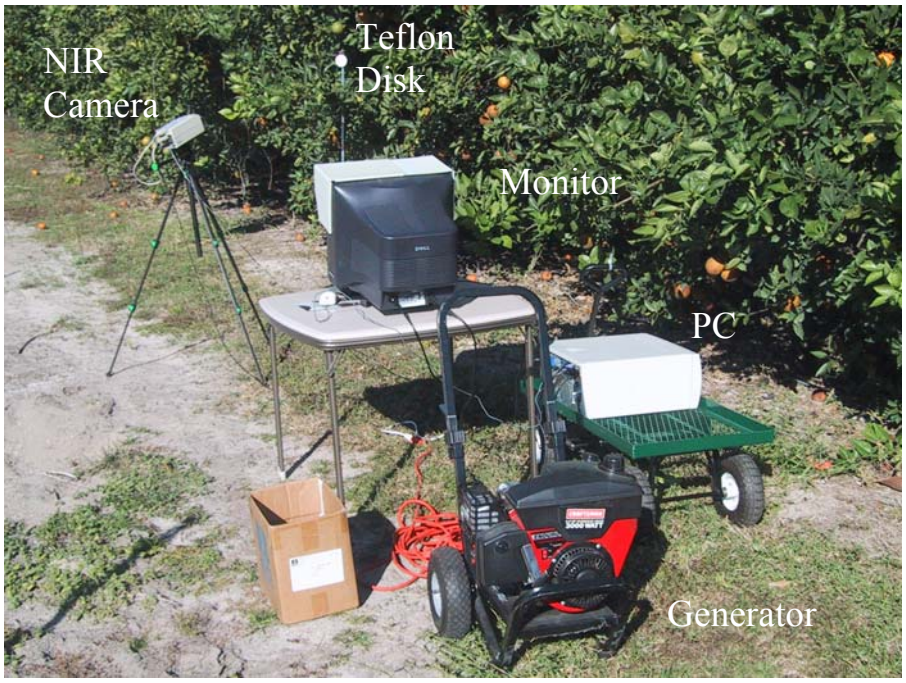


Figure 4-5. In field experimental setup with gasoline generator, personal computer, monitor, NIR camera on tripod, and Teflon disk (from foreground to background).

Preliminary test images were acquired outside in a controlled environment before taking the system to the grove. This was to test the system and handling of the optical equipment before being isolated in a citrus grove. Thirty-six images were acquired at the University of Florida Citrus Research Grove in Gainesville, FL for in-field testing of the multi-spectral imaging system. Target citrus trees were all Hamlin variety. Both the test images and in-field images were acquired in November 2006 under sunny weather conditions. A total of 552 raw images were obtained.

The predetermined experimental plan included a Teflon disk or sheet to be used for raw image light intensity normalization. However, the brightness of the Florida sun saturated the Teflon material in the raw monochromatic images (refer to raw images of Figures 4-9A, 4-10A, or 4-14). Efforts to limit the light to the camera by closing the NIR camera iris and/or shading the Teflon or target area limited the visibility of the fruit and leaf targets. Raw images with the Teflon were used in the study; however, the Teflon was ignored.

**Image Processing**

Results from in-field image acquisitions were treated as a series of three-dimension matrix values. The x- and y-axes formed the two dimensional image while the z-axis was the number of images at the target. This z-axis is also referred to as an image block depth. The z-axis length varied among images depending on the total number of raw images gathered from the target. It was essential for this research that each image block included at least three raw images: one at each of the band pass filters (1064 nm, 1150 nm, and 1572 nm). In every image block studied one raw image for each band was selected for image processing based on image clarity, alignment, and brightness. When only images of each spectral band are used to create an image block it is known as a spectral image block (Gonzalez, et al., 2004). Figure 4-6 shows an example of a spectral image block used in this study.

Image processing was conducted using MatLab 7.0 software with the Image Processing Toolbox (MATLAB, 2006). Raw images were treated as 480 x 640 two dimensional matrices consisting of 8-bit unsigned values. All image processing techniques and mathematical calculations preformed between raw images were computed on a matrix point by point (pixel by pixel) format.

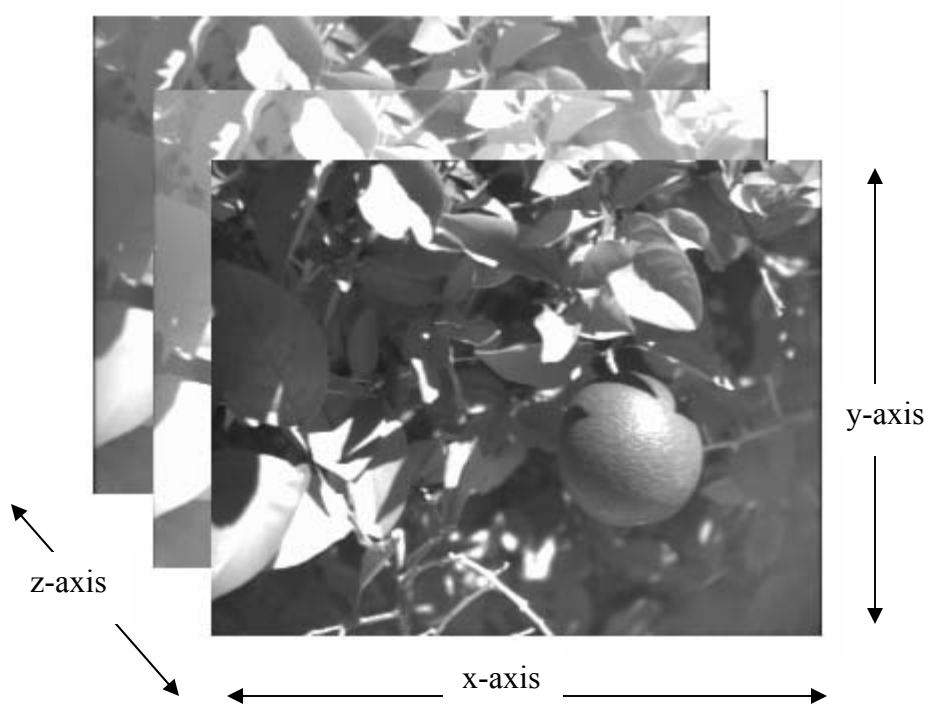


Figure 4-6. Representation of an image spectral block.

**Image processing's major stages**

The image processing steps used in this study consisted of two major stages, each having sub-steps. The two major stages will be referred to as Image Indexing and Marker Checking. In the Image Indexing stage a likelihood image was calculated of each pixel being one of two classes, either citrus fruit or non-citrus fruit. It should be noted that not every pixel is either citrus fruit or citrus leaf as images include branches, sky, ground, Teflon, metal pole or other non-fruit objects; all these possible non-fruit objects are referred to as non-fruit, as it is the desire of this image processing to not count them as citrus fruit. Likelihood images were created based on pixel values of each band pass image. Using Otsu's method, a threshold value was found and each pixel was classified as either citrus fruit or non-citrus fruit. In the Marker Checking stage, a calculation from the original raw images was used to check the validity of the citrus fruit markers, or pixel groups, identified as possible citrus fruit pixels. This calculation was based on

the regional variances which describe the complexity of the image marker. A more complex, thus higher variance region is more likely to be leaves or branches intertwined while a citrus fruit will be less complex. The stages will now be discussed in more detail.

**Image Indexing stage**

The first image processing step of the Image Indexing stage is a simple histogram stretching in order to maximize the reflective light intensities of the monochromatic images. This assures that 1) the maximum amount of data can be extracted from each image and 2) images to be indexed together are at about the same image brightness level. In a histogram stretching process the maximum ($i_{max}$) and minimum ($i_{min}$) pixel value of each image is found. Then each pixel value is multiplied by an enhancement multiplier, $M$, defined in equation 4-1. The result is rounded to the nearest whole number while remaining in the range of 0 to 255.

$$M = \frac{255}{i_{\max} - i_{\min}} \tag{4-1}$$

Where, $i_{max}$, $i_{min}$ = maximum and minimum pixel value, respectively.

This histogram stretching allows overly dark or bright images to use a wider spread of pixel values enhancing the quality of the image as displayed in Figure 4-7. This same process is used again at a later step of the Image Indexing stage.

The second step of the Image Indexing stage was the use of an image smoothing filter. Smoothing filters, also known as image smoothing functions, can be very complex and powerful or quite simple. The resulting smoothed image requirements decide what type of smoothing filter should be used (Gonzalez et al., 2004). Because clear grove images are desirable in this research, a small 3 x 3 pixel smoothing filter using an averaging function was used. The filter is defined mathematically by equation 4-2.

$$P_{i,j} = \left(p_{i-1,j-1} + p_{i-1,j+1} + p_{i+1,j-1} + p_{i+1,j+1} + 3p_{i,j-1} + 3p_{i,j+1} + 3p_{i-1,j} + 3p_{i+1,j} + 8p_{i,j}\right)/24 \tag{4-2}$$

Where, $p_{i\,j}$ = raw image pixel *(i, j)*

$P_{i,j}$ = resulting image pixel *(i, j)*

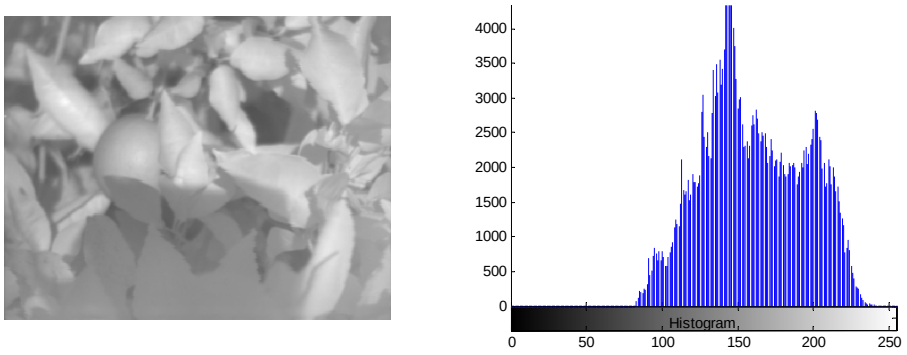


A

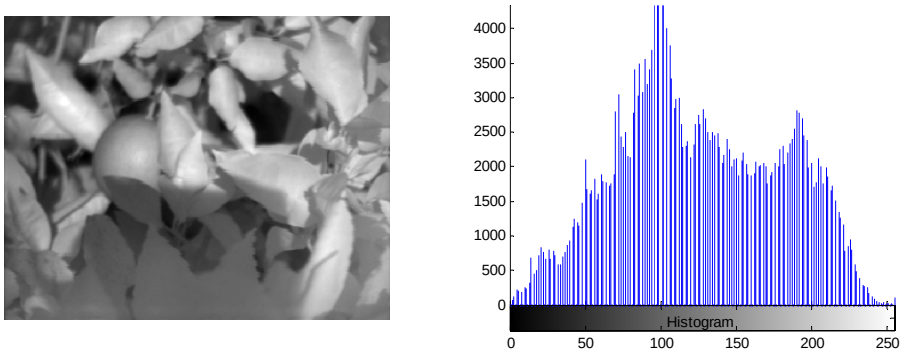


B

Figure 4-7. Histogram stretching function; raw image and histogram A) Before histogram stretching. B) After histogram stretching.

The smoothing filter performed three tasks for improving the image to image calculations: 1) removed random noise in the images; 2) allowed image target edges to smooth the transition between the background and foreground, helping resolve situations where targets did not align perfectly between raw images; 3) extracted information from saturated pixels (i.e., a pixel of 255 located next to pixels of less than 255 was not considered as bright/saturated as a pixel totally surrounded by other saturated pixels of value 255).

The critical image processing step of the Image Indexing stage was the actual index itself. To identify the citrus fruit, an index calculation using all three band pass images was designed.

Indices in remote sensing applications are the mathematical calculations of different spectral band images. Most often in agricultural applications these calculations are preformed with high spatial resolution images acquired by aerial or satellite based systems. The most widely used index is the NDVI or Normalized Difference Vegetation Index (Morgan and Ess, 2003). The use of diffuse reflectance information from Chapter 3 was used as a guide, but image investigations revealed that in-field lighting and target orientation conditions created very different reflectance values than had been expected. Many index calculations were attempted without quality outputs. Examples include ratio indices (such as the 1064 band pass divided by the 1572 band pass; both normalized and un-normalized), indexing by way of finding class likelihoods using Fisher linear discriminant analysis (FLDA) as described in Chapter 3, and even more complex hybrid indices (using multiple indices while solving for the average). When studying the common and reliable spectral indices used in agricultural application the most widely used indices appear very simple (Apan et al., 2003). Further study of the literature inspired the design of the index used in this thesis research. The equation for the index is shown in equation 4-3.

$$B = (b_{1064} / b_{1150}) - (b_{1572} / b_{1150}) \tag{4-3}$$

Where, $b_{1064}$ = images with 1064 nm band pass filter

$b_{1150}$ = images with 1150 nm band pass filter

$b_{1572}$ = images with 1572 nm band pass filter

This green citrus index functions by solving the differences between the reflectance of leaves and citrus fruit at 1064 nm and 1572 nm, but first the images are normalized by the 1150 nm band where the leaves and citrus fruit reflectance are very similar. This normalization eliminates the effects of dark images of one band being indexed with light images of the other band. This index does not represent the ideal segmentation system that was calculated in

Chapter 3 but still uses an interpretation of it. The higher reflectance of the citrus fruit versus citrus leaves around 800-1100 nm is directly compared against the lower reflectance of the citrus fruit versus citrus leaves around 1500-1800 nm. Two critical band pass filters are used, as was desired and a third band pass filter normalizes the image shadows and bright reflections.

The resulting two-dimensional image from the green citrus index can be understood as a pixel likelihood for each class, where high values are citrus fruit and low values are non-citrus fruit. One problem remaining in this likelihood image is that misaligned images can result in pixel calculations being too high; therefore an upper value cut-off was set to 165. This value selection was based on training image histograms. The pixels that exceeded this upper value of 165 were by default set to zero, therefore eliminating them from being classified as citrus fruit pixels. A fine example of this can be seen in the index images (Figure 4-8B and Figure 4-9B), where the brightest spots are not the fruit but the edges of objects which are not properly aligned. The histogram stretching function was used again after this upper value cut off to maximize the pixel value separation for the next threshold step utilizing Otsu's method.

Otsu's method automatically chooses a threshold based on the histogram of a grayscale image (Otsu, 1979). The method is based on discriminant analysis, as discussed in Chapter 3. The objective of such an analysis is to separate each pixel into one of two classes, $C_0$ or $C_1$, based on a threshold value, $t$. Assume $C_0$ represents lower pixel values $\{0, 1, 2, 3, \ldots, t\}$ and $C_1$ represents higher pixel values, $\{t+1, t+2, t+3, \ldots, L-1\}$, where L is the number of grayscale values. Let $\sigma^2_b$ and $\sigma^2_d$ be the between-class variance and within-class variance, respectively. The ideal separation threshold can then be obtained by maximizing the separation of the histogram. The objective is to maximize the ratio of the between-class to within-class with respect to the threshold level, $t$. This is found by stepping through all intensity levels of the

grayscale image and at each level calculate $\sigma^2_b/\sigma^2_d$. The higher this ratio is, the stronger the pixel class separation. MATLAB 7.0 has an Otsu function built into the image processing toolbox (MATLAB, 2006). The function returns only the recommended threshold value and has no effect on the original grayscale image. Otsu's value can be multiplied by a scaling factor lowering or raising the threshold and provided an opportunity to fine tune the method for this citrus image application. The training images showed better classification results with a multiplier value of 1.5. This is due to the citrus images needing a threshold for only the highest valued pixels, as most pixels were non-citrus fruit pixels.

The final step of the Image Indexing stage was to improve the binary image, removing holes and noise using a ten pixel sized 'disk' for erosion then dilation, also referred to as opening (Gonzalez et al., 2004). The selection size of ten pixels was a choice based on the training images. It is feasible to use a larger disk shape and this would improve some results by clearing out medium sized errors, however some images would have all the possible fruit pixels eliminated as well. Again, the MATLAB image processing toolbox has a function for this morphological process (MATLAB, 2006). The complete step by step process of the Image Indexing stage is shown in Figures 4-8 and 4-9.

**Marker Checking stage**

Examination of the final images reveal several extra large and small fruit markers, which was defined as groups of possible citrus fruit pixels in the images. If each marker signals a citrus fruit location in the image, then most images have too many such markers. The Marker Check stage is a means of going back to the 1150 nm band pass image and checking if the marker in the final image makes sense. This is accomplished by treating each marker as a separate feature and checking it individually based on the variance of the pixels in the marker with respect to the number of pixels making up the fruit marker. The 1150 nm band pass image is not the raw

A

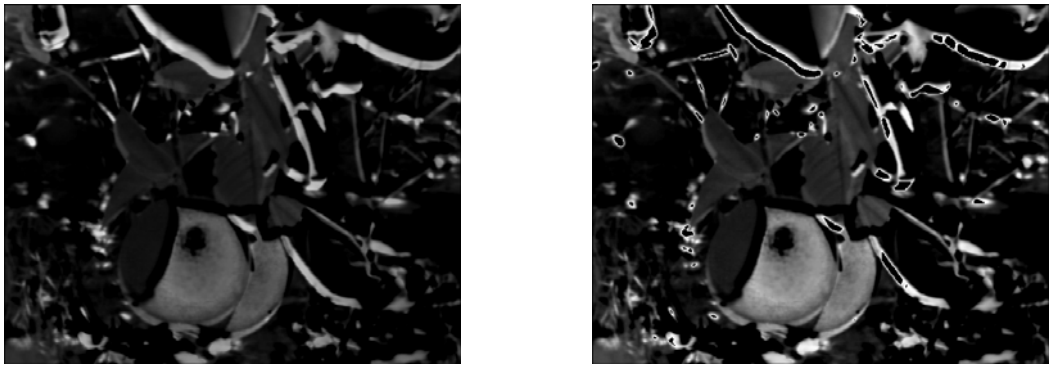

B C

D E

Figure 4-8. Image Indexing stage of validation image number eight. A) Three band pass images 1064 nm, 1150 nm and 1572 nm, respectively. B) After smoothing, histogram stretch and the index calculation steps. C) After upper limit cut off and histogram stretching. D) After thresholding using Otsu's method. E) Final binary image after the use of a 10 pixel erosion and dilation 'disk'.

A

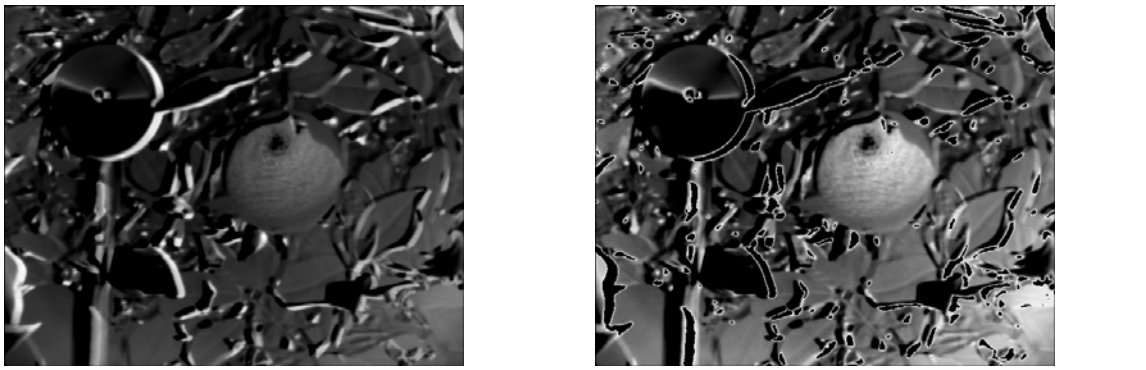

B C

D E

Figure 4-9. Image Indexing stage of training image number 11. A) Three band pass images 1064 nm, 1150 nm and 1572 nm, respectively. B) After smoothing, histogram stretch and the index calculation steps. C) After upper limit cut off and histogram stretching. D) After thresholding using Otsu's method. E) Final binary image after the use of a 10 pixel erosion and dilation 'disk'.

image, but saved after being histogram stretched and smoothed in the Image Indexing stage before being used again in this stage. This prevents noise from negatively affecting the variance calculation results.

The first step of the Marker Checking stage consisted of a simple separation of the markers based on connectivity. If a non-breaking line could be drawn around the marker and connected to the starting point of the line without crossing over another marker or being inside another marker, the enclosed marker would be identified. The next step calculated the distance between the highest and lowest pixel values of the marker and divided it by the total number of pixels, *n*, in the marker. The result is defined as the marker value for that marker, defined in equation 4-4.

$$MV = (p_{\max} - p_{\min}) / n \tag{4-4}$$

Where, $MV$ = marker value

$p_{\max}$, $p_{\min}$ = maximum and minimum pixel values, respectively

$n$ = number of marker pixels

Markers with an *MV* value greater than 0.2 were assumed to be non-citrus fruit markers and were eliminated from consideration. The *MV* value used in this step was chosen based on the trial and error and best results from the training images. It can be interpreted that for every 100 pixels of the marker, a 20 pixel level change was allowed without the marker being removed. The *MV* used was for image processing can be considered conservative, as it permitted some small non-fruit marker errors to be kept rather than risk removing a large correct citrus fruit marker. This major stage also filled any holes in the citrus fruit markers, such as the one seen in Figure 4-10. This *MV* concept was based on the major assumption that leaves, branches, Teflon sheet edges, and other non-citrus fruit objects are more likely to have edges appear in the markers. These edges will have a higher variance in pixel values ranging from the shadow to a

bright glare within a short range. Citrus fruit objects on the other hand tended to have a smoother and less severe rapid change in pixel value. Additionally, because of the method in

A

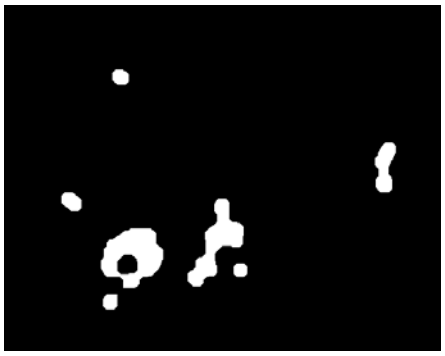

B

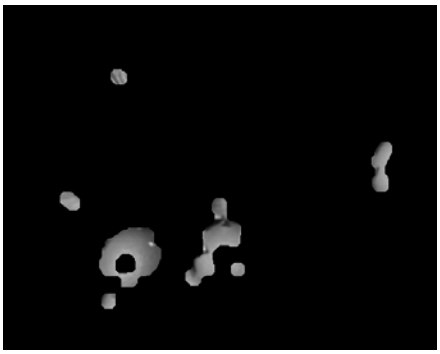

C

D

Figure 4-10. Marker Checking stage of validation image number nine. Input binary image of possible fruit markers (A). The 1150 nm band pass image (B). Markers and the pixel value intensities (C). The new binary image output after removal of most non-fruit markers and filling of marker hole (D). Of the five output fruit markers four are correctly identified as citrus fruit.

which the *MV* is calculated, only smaller markers are at real risk of being eliminated. This means correctly identified citrus markers that include both the dark shadowy edge and the bright sunny spot of the citrus fruit would not be removed as long as the marker size is sufficiently large. On the other hand, small markers are at great risk of being removed and sometimes even correct markers were removed, as in the Figure 4-10. The small marker on the bottom left is incorrectly removed by the Marker Checking scheme, however, an incorrect marker was

removed as well. This type of scheme balances the pros and cons to make images improvements, and for most of the training images the positives outweigh the negatives.

The complete image processing routine involved two major stages, ten sub-steps, and three raw image inputs to produce one final output image. This included variables that were fine tuned by the training image data set. Variables included: smoothing filter type, Otsu's method multiplier of 1.5, upper value cut off of 165, dilatation and erosion 'disk' size, and *MV* limit of 0.2. Slight changes to any one these variables would result in different binary image results. Figure 4-11 is a flow diagram of the complete image processing major stages and sub-steps.

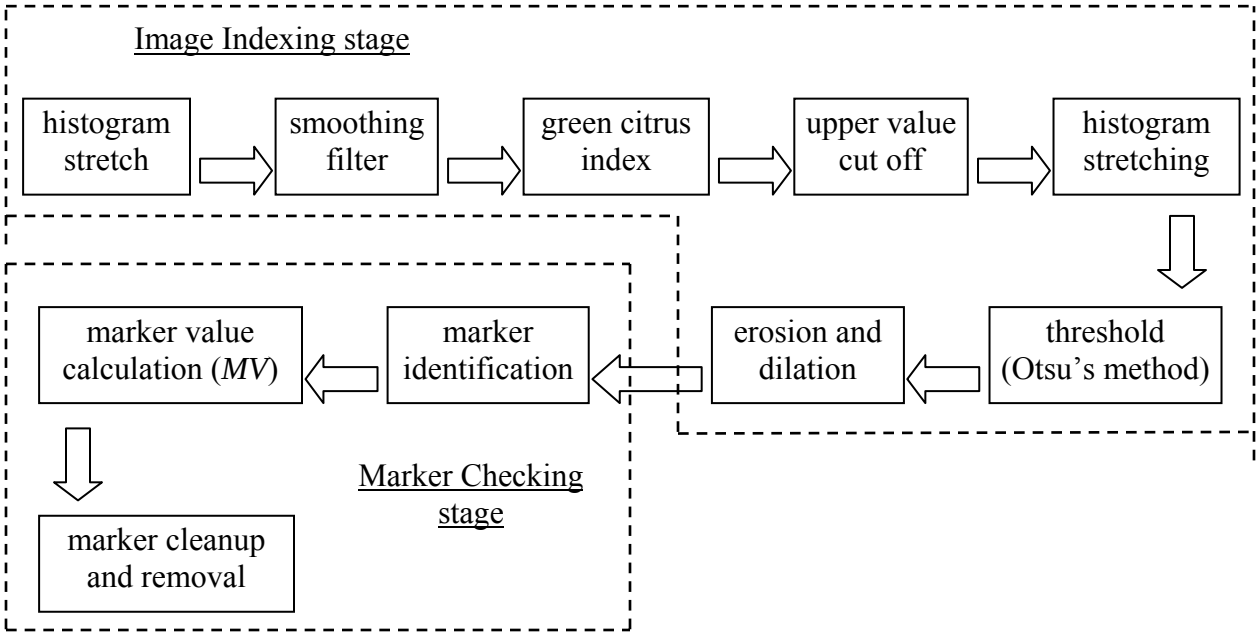


Figure 4-11. Complete image processing procedure.

**Result analysis**

Of the 36 in-field images, two-thirds were randomly selected and used as training data, while one-third was used as validation (i.e., 24 training and 12 validation images). Training images were used in this study to permit the testing of image processing techniques on some images while not being the same images final results would be taken from. This prohibits the

image processing steps from being overly designed and conditioned to the validation images. At the conclusion of the image processing steps each validation image was checked for three measures of accuracy; percent of correct pixels, fruit pixel counts and number of markers. Percent of correct pixels and the fruit pixel counts were measured against manually produced image masks of each validation image showing the citrus pixels (Figure 4-12). The measure of fruit markers is compared to the number of fruit seen by human observation in the images and the number of fruit markers in the manually produced image masks.

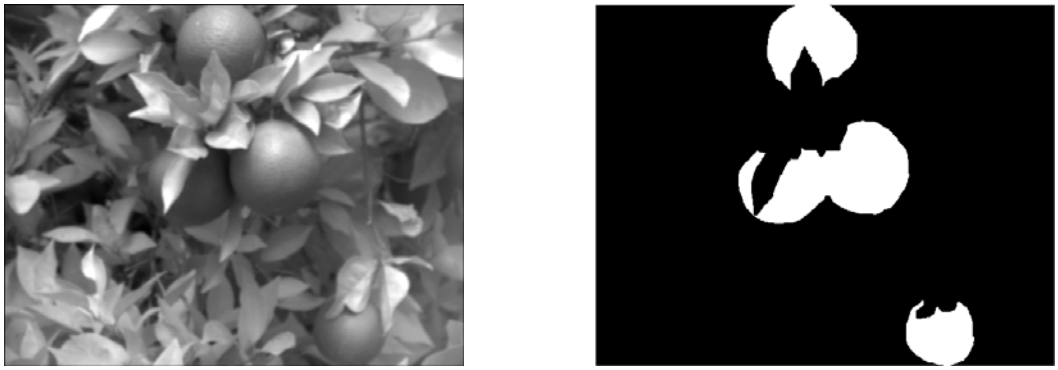

A B

Figure 4-12. Manually produced image mask showing the difference between citrus fruit pixels and non-citrus fruit pixels.

Percent of correct pixels were measured on how many pixels of each image were correctly classified and how many were incorrectly classified. The resulting classifications were judged using Bayes error rate, defined in equation 4-5 (Duda et al., 1988). There are two possible misclassifications: either a pixel $x$ falls in $R_2$ (non-citrus fruit) while its true state of nature is $w_1$ (citrus fruit) or the pixel $x$ falls in $R_1$ (citrus fruit) while its true state of nature is $w_2$ (non-citrus fruit). Otherwise, the classification is defined as correct.

$$P(correct) = 1 - P(error) = 1 - [P(x \in R_2, w_1) + P(x \in R_1, w_2)] \quad (4\text{-}5)$$

Where, $R_1$, $R_2$ = regions 1 (citrus fruit) and 2 (non-citrus fruit)

$w_1$, $w_2$ = classes 1 (citrus) and 2 (non-citrus fruit)

The measure from Bayes error rate (equation 4-5) is out of a probability factor, meaning a perfect 100% rate would be 1.0, while a 50% rate is valued 0.5. In the results section, these unit rates will be discussed in percent correct and percent error.

Image processed fruit pixel counts were measured with respect to the manually masked fruit pixel counts. For each of the 12 validation images used in this study a count of citrus fruit pixels was made from the resulting processed image and the manually masked image. An $R^2$ value was calculated for a linear approximation relating the two measures. This is a very important measure as it provides a quantitative value of the ability to predict the density of green citrus in each image using this method. This is a methodology future researchers could use in determining green citrus yield.

Lastly, a survey was conducted regarding the number of citrus fruit markers found, manually counted number of citrus fruit, and the masked image citrus fruit markers. This is important as it has been the measuring tool of previous research for on-tree citrus fruit identification (Annamalai et al., 2004; Chinchuluun and Lee, 2006). The results conclude with a discussion about the value of such marker count information.

## Results and Discussion

### Image Acquisition Problems

There were many problem that appeared early during the in-field image acquisition process, but there was very little that could be done at the time. These problems and their effects on the results will be discussed before the qualitative results section. The most important issues faced with this experimental design were target shifting, light/shadow changes, raw image saturation and multiple leaf reflections increasing the expected diffuse reflectance.

During the time it took to change out one optical band pass filter for another (30-45 seconds) slight changes could occur in the uncontrolled environment. The two most prevalent

changes were what is referred to as target shifting and light/shadow alterations. While one image may be taken under ideal conditions, subsequent non-ideal conditions could follow closely. This includes the biggest in-field problem of strong breezes shifting the leaves and/or branches and even swinging the target fruit(s) between image acquisitions. Without the fruit being perfectly aligned from one band pass image to another, incorrect edge classification will occur. Figure 4-13 is an example of a target fruit and surrounding branches and leaves shifting as a result of wind turbulence. The two images were taken with the same band pass filter only two or three seconds apart, however, the location of the fruit and leaves shifted dramatically. This problem can not be resolved by a simple shifting of the image to align the fruit, because not all the objects are shifted by the same amount. For example, the leaves just above the Teflon sheet in Figure 4-13 are at approximately the same location in both images. These means a dynamic shifting would need to be used, stretching and compressing different parts of the images to better align them. Such a complex process would become increasingly difficult on such a complex background.

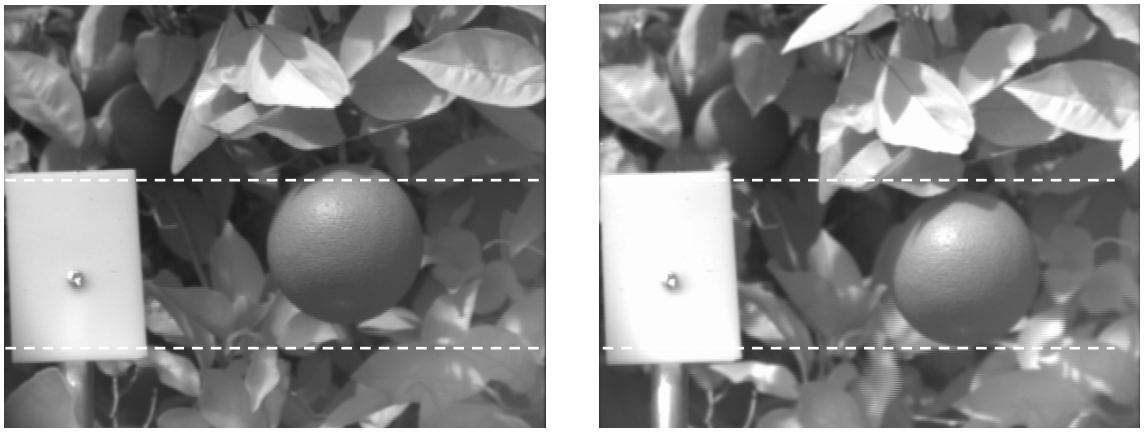

Figure 4-13. Location of the target fruit and some of the leaves has shifted between the two raw images. The Teflon sheet and some leaves remain in the same place.

In addition to wind moving the target and the resulting shadows, shadow and sun illumination changed during image acquisitions due to inconsistent cloud cover and the slow shifting of the sun. These shifts in the sun's location in the sky creates more than a change in

shadow location. The shift changes the solar angle which may affect the magnitude of resulting fruit and leaf reflectance (Gilabert and Melia, 1993). Because raw images at each target location were taken within a short period of time these solar angle effects were not considered in individual images blocks, however it may be a concern if future systems require images to be acquired all day. The only solution used for this research during image acquisition was to take many images quickly and select the images that facilitated better image to image comparisons based on target fruit and/or leaf alignment.

Another major problem during image acquisition was raw image saturation. Many of the images became too dark or too bright. This was most prevalent on the outer and inner layers of the citrus canopy where lighting conditions could vary dramatically. Figure 4-14 shows one example of the light saturation among the leaves and part of the citrus fruit. This was a critical issue as information at these pixels was lost and comparisons to the reflective behaviors of the other wavebands would not be correct. The Teflon sheet in several of the images became the most susceptible to this problem. This is why the use of the Teflon sheet was suspended when it became apparent that the material was too reflective to be used as a normalization material in sunlight.

Figure 4-14. Lighting condition extremes (blackout and saturation) from inside and outside the citrus canopy.

The effects of the saturated pixels are dramatically observed in the histograms; Figure 4-15 shows two images of the same targets using the same band pass filter. They were taken moments apart when the strength of sunlight changed dramatically due to sudden cloud cover. The histogram on the left has around 30000 pixels saturated with a value of 255. The histogram on the right has only about 700 pixels saturated. Comparing these values to the total number of pixels per image (307200 pixels), a loss of almost 10% of the pixels is experienced by the image on the left as apposed to less than one quarter of one percent on the right. During the image acquisition process the mechanical iris of the NIR camera was not precise enough to correct all lighting problems.

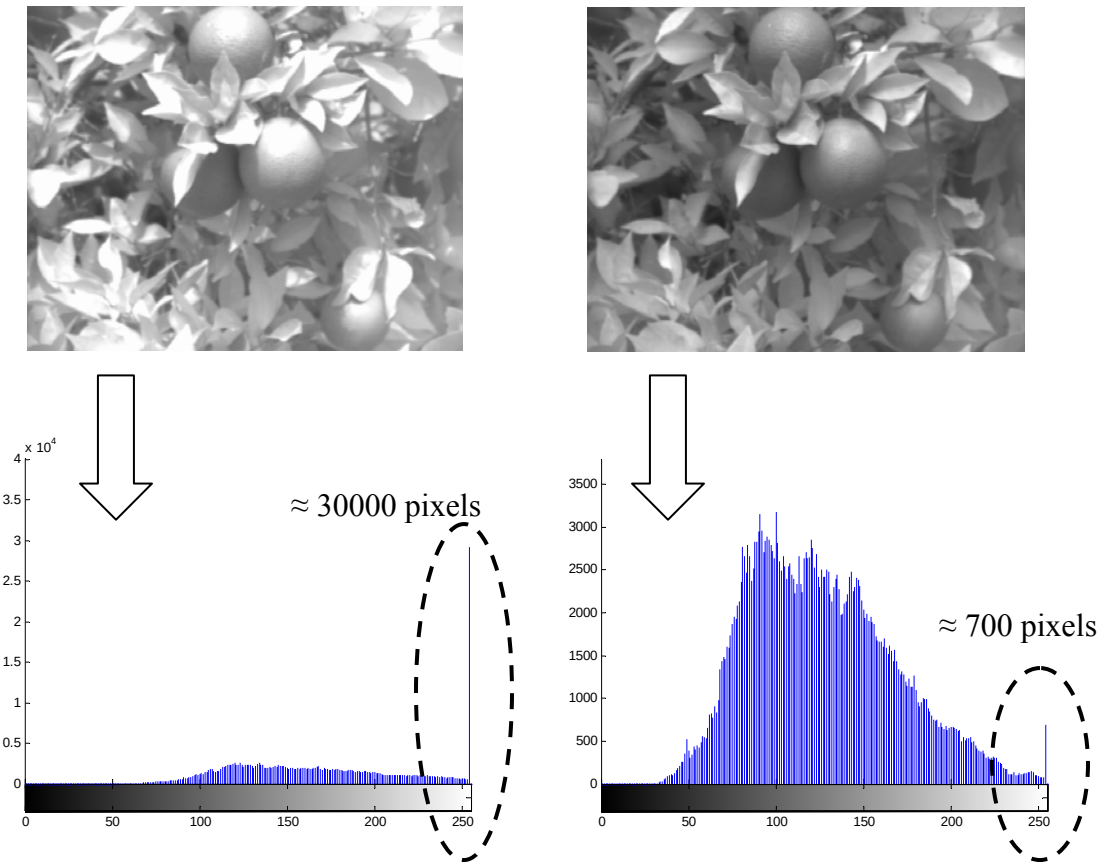


Figure 4-15. Changes in sunlight and the effect on image histograms.

The last issue faced in the experimental setup was foreshadowed in an experiment discussed in Chapter 3. The diffuse reflectance of multiple leaves stacked together were measured with a spectrophotometer (Cary 500, Varian, Inc., Palo Alto, CA) and revealed as the number of leaves increased so did the percent of diffuse reflectance. It was theorized that additional leaves became a second, or third, reflective surface for light waves that passed through the first leaf. After reflecting off the second (or third) leaf, the light would transmit back through the first leaf again, and be detected as light reflected from the first leaf. The acquired NIR camera images show a similar phenomenon as the 1064 nm band images showed only a minor intensity difference between fruit and leaves. In addition, leaves in the NIR camera images were not facing flat but had more variations in direction, which changed the reflectance among leaves and altered the expected reflectance from Chapter 3.

**Quantitative Identification**

Using the image processing methods and variable values described previously, the average correct pixel classification was 90.3% with respect to the manually masked images. Correct pixels were any pixels that had the same classification in the masked image and image processed image. The total number of correct pixels was then divided by the total number of pixels, 307200, to find the percent correct. This is presented in Table 4-2, with a fruit pixel count from the image processing and the masked images. Notice, being able to predict the pixels classification may not the best measure of identification. This will be discussed in more depth in a little bit.

The image processing citrus pixel counts and manually masked citrus pixel counts are also presented in Figure 4-17. Each show the complete number of fruit pixels counted in the results. This count and be interpreted as a type of yield data set for each image. While the sizes of the fruits in each image are not always the same and the distances of the camera to the targets are

variable, the total number of citrus fruit pixels does provide some information. The ability of the image processing algorithm to detect this can be studied using a t-test and solving an $R^2$ for the two data vectors.

Table 4-2. Validation image citrus fruit pixel results.

| Validation image number | Correct pixel classification (%) | Image processing fruit pixel count | Manually masked fruit pixel count |
|---|---|---|---|
| 1 | 94.8 | 1524 | 16624 |
| 2 | 96.9 | 9753 | 18716 |
| 3 | 77.5 | 35756 | 33861 |
| 4 | 96.1 | 1699 | 13084 |
| 5 | 81.9 | 23507 | 63607 |
| 6 | 95.1 | 5936 | 17109 |
| 7 | 82.3 | 4029 | 36512 |
| 8 | 92.9 | 11065 | 31841 |
| 9 | 89.5 | 11001 | 38565 |
| 10 | 97.9 | 1207 | 2733 |
| 11 | 88.1 | 12743 | 36706 |
| 12 | 90.2 | 9550 | 31901 |
| average | 90.3 | 9812.3 | 27538.3 |

Using a two sided t-test to assess the significance of the error percent when comparing image processed fruit counts with manually masked fruit counts, in this case a highly significant difference was found. The p-value was solved to be $4.295 \times 10^{-4}$ making it far too small, which shows the "null hypothesis" to be invalid for this data set. In effect, the t-test results are saying the image processing method was unsuccessful, but only if it is assumed that the manual masking method is defined as a correct reference. Again, the validity and limited usefulness of the manually masked images for checking will be discussed in more depth later.

The two sided t-test method also tested for the equality of variances in the two data sets. The probability was solved as being greater than 0.10, meaning the t-test was valid for the "null

hypothesis" of equal variances. The calculated variance for the image processing vector is $1.0190x10^8$ while being 2.5317x108 for the manually masked images. In addition, the t-test revealed the t-statistic is 4.9590 on 11 degrees of freedom.

Using the image processing techniques and variables discussed previously, the image processing results underestimated the citrus pixel counts for all validation cases. This makes sense when observing the image results in Figures 4-19, 4-20, and 4-21, but can be proven by looking at the data presented in Figure 4-16. A list of four classes based on image processing pixel classification and manually masked pixel classification is given for all 12 validation image. The image processing pixel classification (vertical location) and the manually masked pixel classification (horizontal location) define which corner the pixel count adds to. This means the top left corner are fruit pixels correctly classified as fruit pixels, bottom left corner are non-fruit pixels incorrectly classified as fruit pixels, top right corner are fruit pixels incorrectly classified as non-fruit pixels, and bottom left corner are non-fruit pixels correctly classified as non-fruit pixels. A total for all the validation images is given at the bottom. There are two important observations to pull from this figure.

First, the great numbers of pixels are classified by the image processing as non-citrus fruit and are manually masked as non-citrus fruit. This is seen by how much larger the value in the non-citrus/non-citrus box is in the bottom right corner. This facilitates for a high percent correct, as in Table 4-2, but does not display true identification.

The second important observation in Figure 4-16, is the relative values of image processing classified non-fruit that are masked as fruit (bottom left corner), versus the image processing classified fruit that are masked as fruit (top left corner). The lower the bottom left corner value relative to the top left corner, the more correct the identification without improper

classification. The best examples of this are validation image numbers one, two, four, seven, nine, eleven and twelve. All these validation images are examples of the image processing finding the citrus fruits but did not completely covering the masked area. For a good example of this, refer to Figure 4-20. The shadowed edges and bright glare of the sun eliminated parts of the fruit from being classified correctly. The image processing algorithm is conservative with the selection of citrus fruit pixels as a way to safe guard against classifying non-citrus fruit pixels as citrus fruit pixels.

Image 1

| | f | n |
|---|---|---|
| f | 1590 | 15917 |
| n | 15 | 289678 |

Image 2

| | f | n |
|---|---|---|
| f | 10265 | 9445 |
| n | 6 | 287484 |

Image 3

| | f | n |
|---|---|---|
| f | 2025 | 33634 |
| n | 35629 | 235912 |

Image 4

| | f | n |
|---|---|---|
| f | 1789 | 11990 |
| n | 0 | 293421 |

Image 5

| | f | n |
|---|---|---|
| f | 18068 | 48916 |
| n | 6687 | 233529 |

Image 6

| | f | n |
|---|---|---|
| f | 4675 | 13343 |
| n | 1576 | 287606 |

Image 7

| | f | n |
|---|---|---|
| f | 11653 | 21879 |
| n | 0 | 273668 |

Image 8

| | f | n |
|---|---|---|
| f | 9908 | 30705 |
| n | 1677 | 264910 |

Image 9

| | f | n |
|---|---|---|
| f | 1590 | 15917 |
| n | 15 | 289678 |

Image 10

| | f | n |
|---|---|---|
| f | 1447 | 5819 |
| n | 524 | 299410 |

Image 11

| | f | n |
|---|---|---|
| f | 12743 | 23963 |
| n | 0 | 264147 |

Image 12

| | f | n |
|---|---|---|
| f | 9495 | 22406 |
| n | 55 | 267603 |

Total of all validation images

| | f | n |
|---|---|---|
| f | 85248 | 253934 |
| n | 46184 | 3301034 |

Figure 4-16. Pixel classification results for all validation images and the overall total. (Notice, top left corner are fruit pixels correctly classified as fruit pixels, bottom left corner are non-fruit pixels incorrectly classified as fruit pixels, top right corner are fruit pixels incorrectly classified as non-fruit pixels, and bottom left corner are non-fruit pixels correctly classified as non-fruit pixels.)

The $R^2$ of all the fruit pixel counts is 0.390 (Figure 4-17). However, it is evident from the graph that the point (35756, 33861) is an outlier. This even more evident from the poor performance of this validation image number three, which is presented in detail in Figure 4-21. If this validation image is dropped, a fruit pixel to fruit pixel $R^2$ of 0.765 was calculated (Figure 4-18). Also the narrowing of the 90% confidence prediction bounds displays this same significance of the outliner removal. The $R^2$ results would be higher if the calculations come from non-citrus pixel counts as most of the images were of non-citrus pixels.

A major question that this research has shown is that of, what is identification? Is the best measure of identification the correct number of pixel counts or the number of markers (or fruit) counted? The problem with counting pixels that are correct or incorrect lies in an example where no citrus fruit pixels are identified by the image processing system. If image processing result predicted zero citrus pixels, the answer would still be over 50% correct for these images used as no image in this study had citrus pixels covering more than half of the image area. But there are also problem with the use of citrus fruit markers to determine the number of citrus fruit, which has been the standard method in previous citrus identification schemes (Annamalai et al., 2004; Chinchuluun and Lee, 2006). While justification of this counting method can be made due to the distance of the camera from the canopy and the resulting number of citrus per image (10 to 50), it should be noted that a citrus pixel marker may not be accurate for other conditions. Close images of a citrus canopy generally lead to problems of over or under estimation of fruit. In the first example, the view of one fruit can be obstructed by a branch. The image processing might work properly and identify the two visible sides independently, thus two markers for one fruit. The second example is a great number of fruits collected together and touching while on the tree. In this case, only one marker is created for two or more citrus fruits. These are pertinent

concerns for a relatively close camera-to-canopy experiment when only a few fruits are visible in each image.

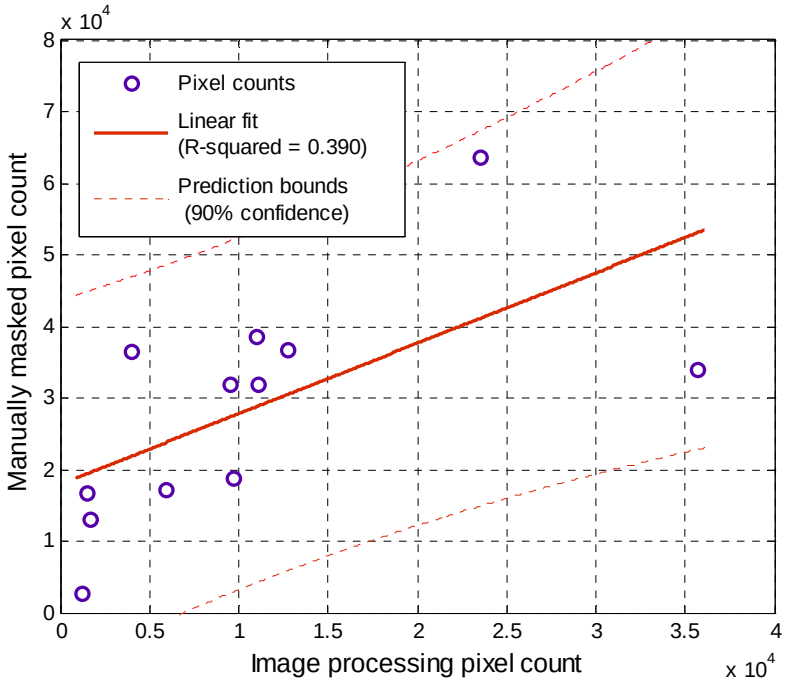


Figure 4-17. Manually masked fruit pixel count versus image processing fruit pixel count results with linear best fit using all pixel count data.

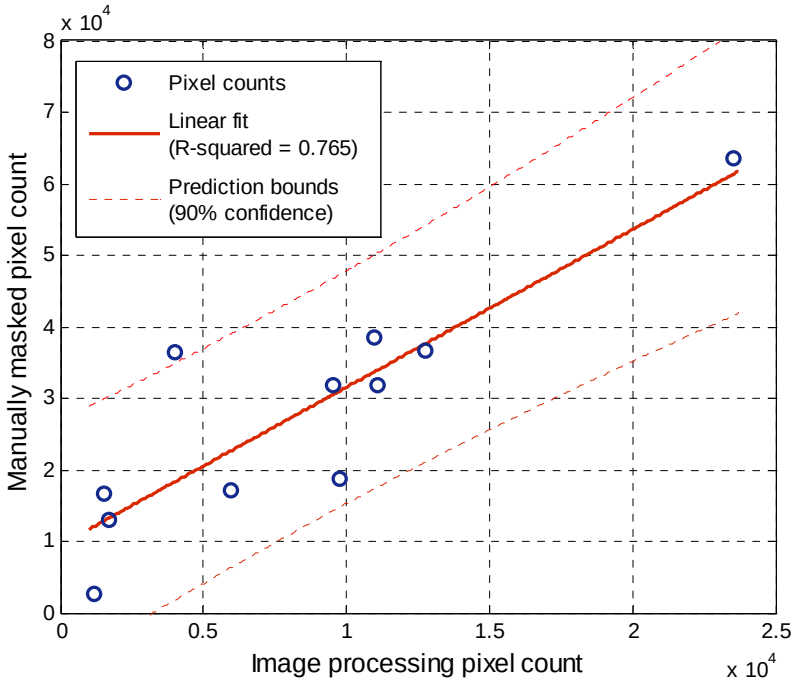


Figure 4-18. Manually masked fruit pixel count versus image processing fruit pixel count results with linear best fit with one outlier removed.

The results from the validation image fruit markers and human fruit counts are listed in Table 4-3. Fruit marker results reveal a stronger correlation between the image processing fruit markers and the actual human observed fruit count. This is primarily due to the second example discussed above; affecting validation images number five and nine the most. There is one case of example one in validation image number four. The image processing fruit marker counts do follow the human observation, but this might only be a result of noisy outputs at coincidentally correct image numbers. There are cases when the extra fruit markers harm the results, such as validation images six and seven.

Table 4-3. Validation image fruit marker and manually masked marker results.

| Validation image number | Image processing fruit marker count | Manually masked marker count | Human observed fruit count |
|---|---|---|---|
| 1 | 1 | 1 | 1 |
| 2 | 1 | 1 | 1 |
| 3 | 5 | 3 | 4 |
| 4 | 1 | 2 | 1 |
| 5 | 8 | 3 | 9 |
| 6 | 4 | 1 | 1 |
| 7 | 4 | 2 | 2 |
| 8 | 1 | 1 | 2 |
| 9 | 5 | 4 | 7 |
| 10 | 2 | 1 | 1 |
| 11 | 3 | 1 | 1 |
| 12 | 4 | 2 | 5 |

Three complete image processing and resulting classifications and misclassifications images are given (Figures 4-19, 4-20, 4-21). These three image results represent typical results in both the training and validation sets. Figure 4-19 shows a very complex grouping of citrus fruit with only shadows in the background. The raw images of the 1064 nm and 1150 nm band pass filters suffer from glare on the right hand side. This creates the incorrect fruit markers on

the right hand side. Six of the nine fruit are marked, with three unmarked, and two image processing fruit markers being incorrect. It is difficult for multiple green citrus fruit to be properly identified together as they never have the same light illumination. This creates unequal ratios between the two key band pass filters, 1064 nm and 1572 nm, which always leave some fruit out or too many non-citrus fruit inside the thresholding boundary.

Figure 4-20 shows a very common single fruit marker identification. In this case the Marker Checking stage is not even necessary. What is interesting about this image is the bright sun spot on the citrus fruit because the loss of data due to saturation at this point prohibits the region from being properly classified as fruit. This "C" shape is quite common and can be closed up if desired. Such an algorithm was not included in image processing because occasionally, as was observed in the training data, a very large "C" can occur when multiple fruit are touching. In that case, closing up the "C" is not desirable. Because of the commonality of this type of image result, the average number of image processed fruit pixels is about one-third that of the masked fruit pixels. This same pattern can be observed in Figure 4-16 with validation image numbers one, two, four, seven, nine, eleven and twelve.

Finally, Figure 4-21 reveals a case of extreme incorrect fruit identification. This is not a result of the image processing algorithm, but the poor quality of images acquired. In this case the band pass at 1572 nm is not dark enough. This makes the raw images of the three band passes too similar and no multispectral information can be obtained. Instead, the green citrus indexing reveals a sight ringing effect which is the result of placing optical band pass filters in front of the focal lens of the NIR camera.

## Conclusions

This Chapter tested a ground based multispectral image acquisition and image processing system for identifying green citrus fruit against a green citrus leaf canopy. The image acquisition

A

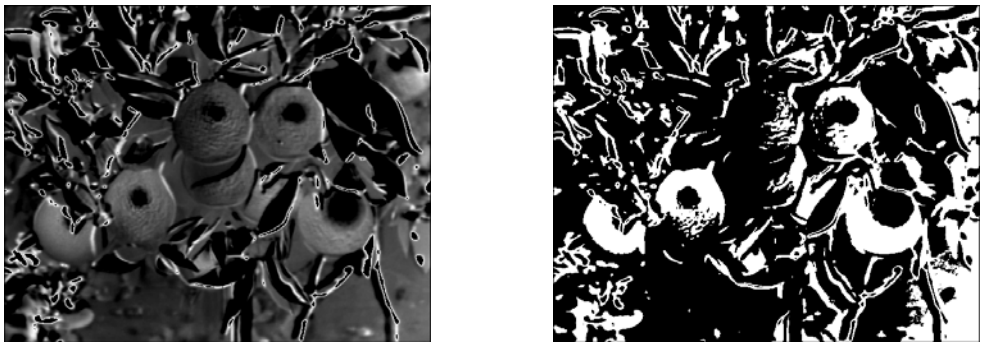

B C

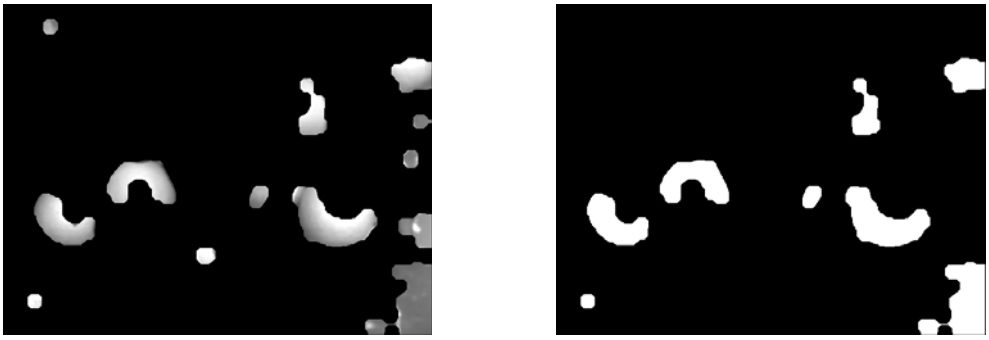

D E

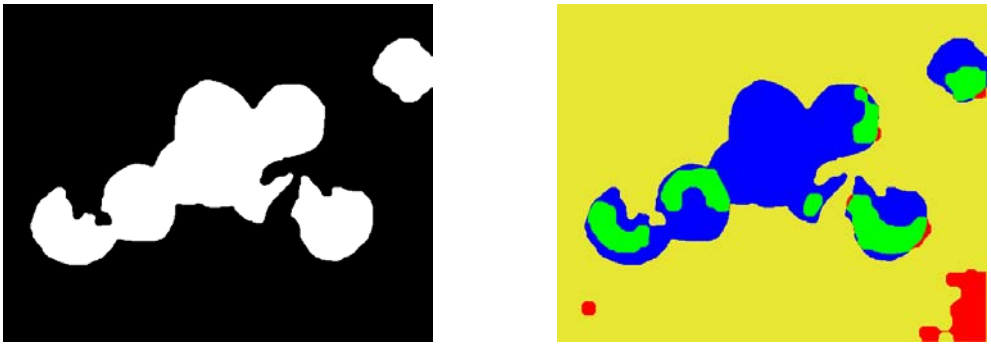

F G

Figure 4-19. Complete image processing and results check of validation image number five. A) Three band pass images 1064 nm, 1150 nm and 1572 nm, respectively. B) Green citrus index, upper limit cut off and histogram stretch. C) Thresholding using Otsu's method. D) Possible fruit markers and the pixel value intensities. E) Marker Checking output binary image. F) Manually produced mask of citrus locations. G) Pixel classifications and misclassifications. Notice, six of the eight fruit are marked, with three unmarked, and two image processing fruit mark being wrong.

A

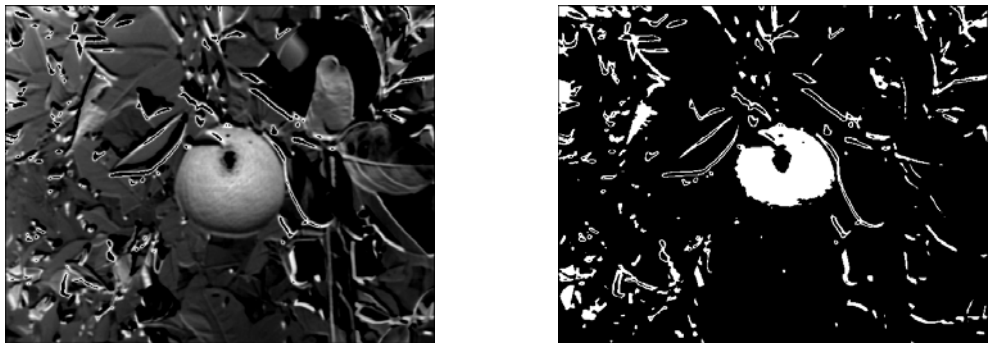

B C

D E

Figure 4-20. Complete image processing and results check of validation image number two. A) Three band pass images 1064 nm, 1150 nm and 1572 nm, respectively. B) Green citrus index, upper limit cut off and histogram stretch. C) Thresholding using Otsu's method. D) Marker Checking output binary image. G) Pixel classifications and misclassifications.

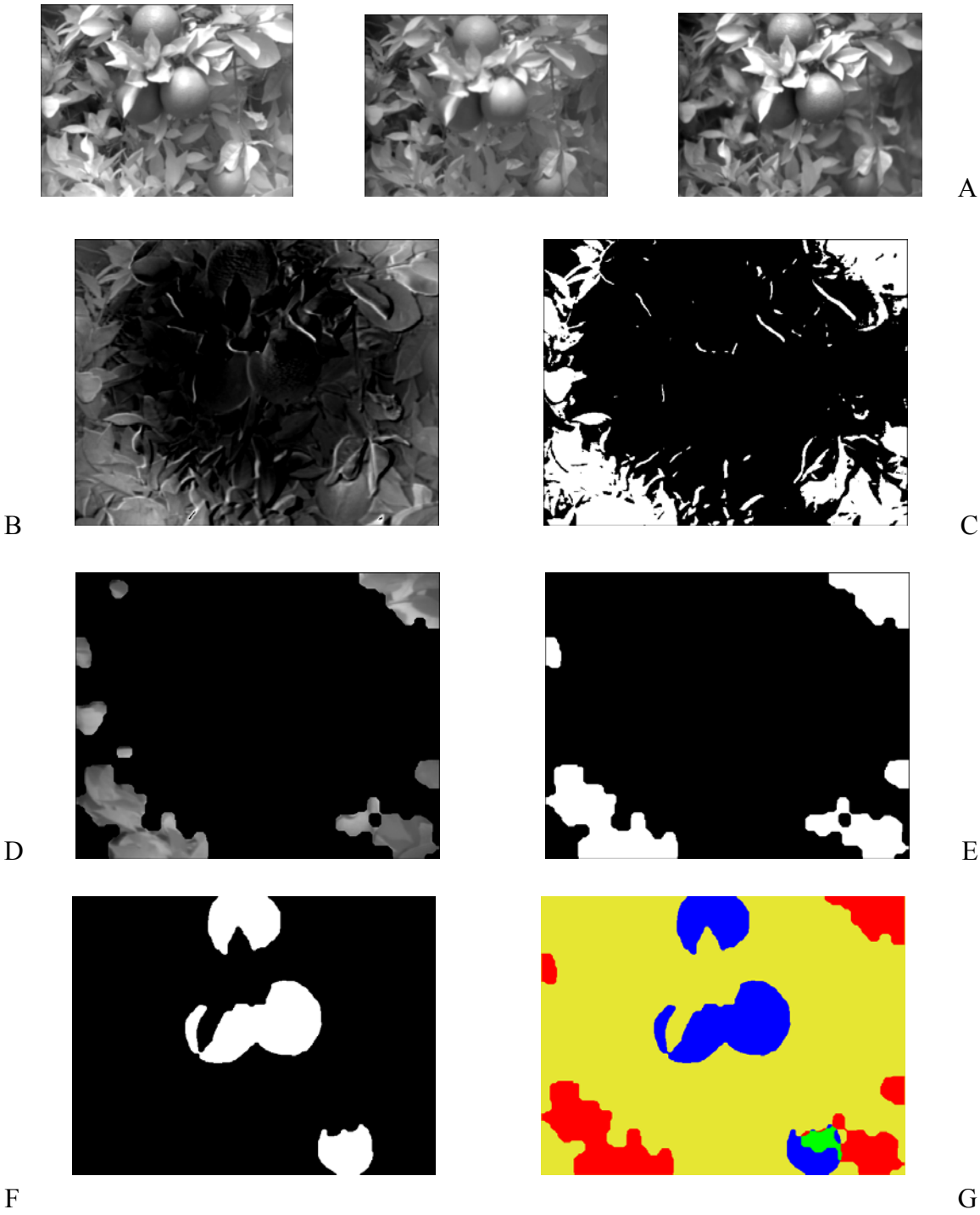


Figure 4-21. Complete image processing and results check of validation image number three. A) Three band pass images 1064 nm, 1150 nm and 1572 nm, respectively. B) Green citrus index, upper limit cut off and histogram stretch. C) Thresholding using Otsu's method. D) Possible fruit markers and the pixel value intensities. E) Marker Checking output binary image. F) Manually produced mask of citrus locations. G) Pixel classifications and misclassifications.

was completed in a Florida citrus grove. A highly sensitive NIR camera was used in conjunction with three optical band pass filters (1064 nm, 1150 nm, and 1572 nm). The resulting images were separated into 24 training images and 12 validation images. A complex image processing scheme was designed involving indexing of the band pass filter images. Measurements of correctness were based on fruit pixel identifications with respect to a manually produced fruit pixel mask.

Quantitative results showed that correct pixel class identification of the 12 validation images was 90.3% when using the image processing algorithm and variable described. When comparing citrus pixel count from the image processing algorithm to the manually masked citrus pixel count, an $R^2$ of 0.764 was achieved with the removal of one outlier. There were a great number of problems during image acquisition that hampered the research in later stages of data analysis. These problems included target shifting, lighting conditions, cloud cover, wind, band pass filter removal, band pass filter alignment, and user mistakes. All of these problems, however, can be summarized as a result of an uncontrollable environment. Despite these problems, the results do prove the effectiveness of the concepts presented in this study. Green citrus fruit can be identified based on spectral differences from leaves by an NIR camera. However, there are still many refinements that require further investigation.

The most important knowledge gathered in this study was a first hand account of technical issues faced and how they might be overcome in future systems. The most import requirements for improved results include the system being capable of acquiring multiple waveband images simultaneously. This would resolve almost all the environmental issues mentioned previously. A second problem researchers would need to solve is lighting conditions. The sun is not a

reliable and consistent light source. It moves through the day, changes intensity based on cloud cover, and cannot penetrate deep into the citrus canopy.

This research goal of this Chapter was to design and test a non-destructive NIR camera based computer vision system for identifying and counting green citrus yield in-field while still on the tree. Results have proved this is possible, but still difficult due to environment conditions and technical difficulties. The last Chapter summarizes this thesis research and discusses what it means for NIR sensing systems in the future.

# CHAPTER 5
# CONCLUSIONS AND FUTURE WORK

## Conclusions of Research Objectives

Near infrared (NIR) sensing technology is a promising, rapidly affordable, and available tool for precision agriculture systems. The non-destructive nature of spectral-based sensing is welcomed by growers who would rather not sacrifice their products. This research has shown that NIR sensors can be used to separate green citrus fruit and green citrus leaves by means of spectral reflectance in the NIR range. This research has proven through the use of training and validation sample sets that perfect separation is feasible using only two wavelengths features (881 nm and 1381 nm). These results were found through the use of the Fisher linear discriminant analysis (FLDA) algorithm for multi-dimensionality breakdown.

This research has also proven that correct identification of citrus fruit is possible using NIR optical equipment. In this research an NIR monochromatic camera was outfitted with three band pass filters (1064 nm, 1150 nm, and 1572 nm). Image processing and multispectral indexing was used to classify the image contents pixel by pixel. By using 24 training images an image processing algorithm was designed and tested. Twelve validation image results showed a 90.3% correct pixel classification (citrus fruit or non-citrus fruit) obtained. In addition, the image processing scheme provided an $R^2$ of 0.746 for fruit pixel counting versus a manually masked fruit pixel count with one outlier data being disposed. Despite these positive accomplishments, this research has shown that better image processing methodologies need to be explored, additional feature NIR spaces should be considered, and the high cost of NIR camera and optical equipment needs to decline for this technology to thrive. Also uncontrollable environmental issues need to be thought through and planned for to improve upon these results.

## Future Work

Highly accurate spectroscopic systems are not currently easy to transport or use in demanding environmental conditions, such as a Florida citrus grove. When smaller and cheaper in-field spectrophotometer systems become more available, the development of nutrient variation maps based on both leaf and fruit samples will be possible. This increase of grove information will provide growers more opportunities to improve their management techniques on grove site-specific basis.

Multispectral NIR cameras can be used for the identification of green citrus fruit in a citrus grove. It is not hard to predict that future research will be more accurate and capable of counting fruit while on the move. Combinations of this system with GPS receivers could create on-the-go citrus yield maps early in the season. This dream system is still a long way off in the future, but this research opens the door to possible uses of remote NIR sensor systems in the Florida citrus industry. It is conceivable that in the future, autonomous VIS-NIR remote sensor guided vehicles could be used to find, count, map, and even test citrus fruit for health and nutrient content, as some research suggests, while in the grove. Such a futuristic system is the ultimate goal of precision agriculture research not only in the Florida citrus industry but all modern agricultural industries.

# LIST OF REFERENCES


Alchanatis, V., Cohen, Y., Cohen, S., Moller, M., Meron, M., Tsipris, J., Orlov, V., Naor, A., Charit, Z., 2006. Fusion of IR and multispectral images in the visible range for empirical and model based mapping of crop water status. ASABE Meeting Paper No. 061171. ASABE, St. Joseph, MI.

Aleixos, N., Blasco, J., Navarron, F., Molto, E., 2002. Multispectral inspection of citrus in real-time using machine vision and digital signal processors. Computers and Electronics in Agriculture 33, 121-137.

Annamalai, P., Lee, W.S., 2004. Identification of green citrus fruits using spectral characteristics. ASAE Meeting Paper No. FL041001. ASAE St. Joseph, MI.

Annamalai, P., Lee, W.S., Burks, T.F., 2004. Color vision system for estimating citrus yield in real-time. ASAE/CSAE Meeting Paper No. 043054. ASAE St. Joseph, MI.

Apan, A., Held, A., Phinn, Markley, J., 2003. Formulation and assessment of narrow-band vegetation indices from EO-1 Hyperion Imagery for discriminating sugarcane disease. Proc Spatial Sciences Conf., 1-13.

Chinchuluun, R., Lee, W.S., 2006. Citrus yield mapping system in natural outdoor scenes using the watershed transform. ASABE Paper No. 063010. ASABE, St. Joseph, MI.

Chinchuluun, R., Lee, W.S., Ehsani, R., 2007. Citrus yield mapping system on a canopy shake and catch harvester. ASABE Meeting Paper No. 073050. ASABE, St. Joseph, MI.

Citrus Research and Education Center (CREC), 2007. Precision agriculture history in Florida. Available at: http://www.crec.ifas.ufl.edu/crec_websites/precision_agriculture/history.htm. Accessed: March 25, 2007.

Ding, P., 2005. Use of Nondestructive Spectroscopy to Assess Chlorophyll and Nitrogen in Fresh Leaves. Unpublished Ph.D. Dissertation. Oregon State University, OR.

Duda, R.O., Hart, P.E., Stork, D.G., 1988. Pattern Classification, 2nd ed. John Wiley and Sons, New York.

Fisher, R.A., 1936. The use of multiple measurements in taxonomic problems. Annels of Eugenics 7, 79-88.

Florida Agricultural Statistics Service (FASS), 2005. Citrus 2004-05 Summary. Available at: http://www.nass.usda.gov/fl/rtoc0ci.htm. Accessed: May 3, 2006.

Fraser, D.G., Jordan, R.B., Kunnemeyer, R., McGlone, V. A., 2002. Light distribution inside mandarin fruit during internal quality assessment by NIR spectroscopy. Postharvest Biology and Technology 27, 185-196.

Gaffney, J.J. 1972. Reflectance properties of citrus fruits. Transaction of the ASAE. 15, 310-314.

Gilabert, M., Melia, J., 1993. Solar angle and sky effects on ground reflectance measurements in a citrus canopy. Remote Sensing Environment 45, 281-293.

Gonzalez, R.C., Woods, R.E., Eddins, S.L., 2004. Digital Image Processing Using MATLAB. Pearson Prentice Hall, Upper Saddle River, NJ.

Grift, T., Ehsani, R., Nishiwaki, K., Crespi, C., Min, M., 2006. Development of a yield monitor for citrus fruits. ASABE Meeting Paper No. 061192. ASABE, St. Joseph, MI.

Gumz, M., Weller, S.C., 2005. Using remote sensing to differentiate weeds in mint. Top Farmer Crop Workshop Newsletter, April.

Jimenez, A.R., Ceres, R., Pons, J.L., 2000. A survey of computer vision methods for locating fruit on trees. Transaction of the ASAE 43 (6), 1911-1920.

Labsphere, 2006. A Guide to Integrating Sphere Theory and Applications. Labsphere Inc., North Sutton, NH. Available at: http://www.labsphere.com/data/userFiles/A%20Guide%20to%20Integrating%20Sphere%20Theory&Apps.pdf. Accessed: Nov 5, 2006.

Lee, W.S., Slaughter, D.C., 2004. Recognition of partially occluded plant leaves using a modified watershed algorithm. Transaction of the ASAE 47 (4), 1269-1280.

MacArthur, D.K., Schueller, J.K., Lee, W.S., Crane, C.D., MacArthur, E.Z., and Parson, L.R., 2006. Remotely-piloted helicopter citrus yield map estimation. ASABE Meeting Paper No. 063096. ASABE, St. Joseph, MI.

MATLAB, 2006. Learning MATLAB 7 Release 14. MathWorks Inc., Natick, MA.

Merzlyak, M.N., Gitelson, A.A., Chivkunova, O.B., Rakitin, V.Y., 1999. Non-destructive optical detection of pigment changes during leaf senescence and fruit ripening. Physiologia Plantarum 106, 135-141.

Min, M. 2006. Spectral-Based Nitrogen Sensing for Citrus. Unpublished Ph.D. Dissertation. University of Florida, FL.

Morgan, M., Ess, D., 2003. The Precision-Farming Guide for Agriculturists. John Deere Publishing, Moline, IL.

Nagy, S., Shaw, P.E., Veldhuis, M.K., 1977. Citrus Science and Technology. Vol. 1. Avi Publishing Co., CT.

Otsu, N., 1979. A threshold selection method from gray-level histograms. IEEE Transactions on Systems, Man and Cybernetics 9 (1), 62-66.

Regunathan, M., Lee, W.S., Annamalai, P., 2005. Green citrus fruit identification using spectral characteristics. 5ECPA-2ECPLF Book of Abstracts, 246-247.

SAS, 2006. SAS 9.1 Software Documentation and Examples. SAS Institute Inc., Cary, NC. Available at: http://support.sas.com/rnd/app/papers/. Accessed November 1, 2006

Schertz, C.E., Brown, G.K., 1968. Basic considerations in mechanizing citrus harvest. Transaction of the ASAE., 343-346.

Sevier, B.J., Lee, W.S., 2003. Adoption trends and attitudes towards precision agriculture in Florida citrus: preliminary results from a citrus producer survey. ASAE Meeting Paper No. 031100. ASAE, St. Joseph, MI.

Sevier, B.J., Lee, W.S., 2004. Precision agriculture in citrus: a probit model analysis for technology adoption. ASAE Meeting Paper No. 041092. ASAE, St. Joseph, MI.

Stajnko, D., Lakota, M., Hocevar, M., 2004. Estimation of number and diameter of apple fruits in an orchard during the growing season by thermal imaging. Computers and Electronics in Agriculture 42, 31-42.

Stajnko, D., Cmelik, Z., 2005. Modelling of apple fruit growth by application of image analysis. Agriculturae Conspectus Scientificus 70, 59-64.

Tabb, A.L., Peterson, D.L., Park, J., 2006. Segmentation of apple fruit from video via background modeling. ASABE Meeting Paper No. 063060. ASABE, St. Joseph, MI.

Tian, L.F., Slaughter, D.C., 1998. Environmentally adaptive segmentation algorithm for outdoor image segmentation. Computers and Electronics in Agriculture 21, 153-168.

Welte, H.F., 1990. Forecasting harvest fruit size during the growing season. Acta Horticulturae 276, 275-282.

Williams, P., and Norris, K., 2001. Near-Infrared Technology: In Agriculture and Food Industries, 2nd ed. American Association of Cereal Chemists, Inc., St. Paul, MN.

Winter, F., 1986. Modeling the biological and economic development of an apple orchard. Acta Horticulturae 160, 353-360.

Whitney, J.D., Wheaton, T.A., Miller, W.M., Salyani, M., Schueller, J.K., 1998. Site-specific yield mapping for Florida citrus. Proc. Florida State Horticulture Society 111, 148-150.

Whitney, J.D., Q. Ling, Wheaton, T.A., Miller, W.M., 1999. A citrus harvesting labor tracking and yield monitoring system. ASAE Meeting Paper No. 993107. ASAE, St. Joseph, MI.

Whitney, J.D., Q. Ling, Wheaton, T.A., Miller, W.M., 2001. A citrus harvesting labor tracking and yield monitoring system. Applied Engineering in Agriculture 17, 121-125.

# BIOGRAPHICAL SKETCH

The author was born in 1981 in Mansfield, Ohio. Most of his childhood was in Melbourne, FL where he graduated from Eau Gallie High School, 1999 and Brevard Community College with an Associate of Arts degree in 2001. In May 2005 he graduated with a Bachelor of Engineering degree in electrical engineering from the University of Florida. Continuing his education, Kevin graduated from the University of Florida in August 2007 with a Master of Engineering degree in agricultural and biological engineering and another Master of Engineering in electrical and computer engineering. Kevin Kane currently lives in Aiken, SC with his loving wife Dr. M. Kane and his two dogs Bailey and Killian.